

Inverse amplitude method in $\pi\pi$ scattering in chiral perturbation theory to two loops

J. Nieves,* M. Pavón Valderrama, and E. Ruiz Arriola†

Departamento de Física Moderna, Universidad de Granada, E-18071 Granada, Spain

(Received 10 September 2001; published 10 January 2002)

The inverse amplitude method is used to unitarize the two-loop $\pi\pi$ scattering amplitudes of SU(2) chiral perturbation theory in the $I=0, J=0, I=1, J=1$, and $I=2, J=0$ channels. An error analysis in terms of the low energy one-loop parameters $\bar{T}_{1,2,3,4}$ and existing experimental data is undertaken. A comparison to standard resonance saturation values for the two-loop coefficients $\bar{b}_{1,2,3,4,5,6}$ is also carried out. Crossing violations are quantified and the convergence of the expansion is discussed.

DOI: 10.1103/PhysRevD.65.036002

PACS number(s): 11.10.St, 11.30.Rd, 11.80.Et, 13.75.Lb

I. INTRODUCTION

The $\pi\pi$ reaction is theoretically one of the cleanest processes in hadronic physics. This is because crossing, unitarity, and analyticity impose severe constraints on the scattering amplitude [1]. Thus, a lot of attention has been paid to the study of this process and the determination of partial wave phase shifts [2–10]. The current theoretical setup for such an approach is chiral perturbation theory (ChPT), which is an effective field theory embodying all these constraints, and leads to a perturbative expansion of the scattering partial wave amplitude in the (I, J) isospin-spin channel:¹

$$t_{IJ}(s) = t_{IJ}^{(2)}(s) + t_{IJ}^{(4)}(s) + t_{IJ}^{(6)}(s) + \dots \quad (1)$$

Here the expansion parameter turns out to be $\lambda^2 \equiv m_\pi^2 / (4\pi f_\pi)^2 \sim 0.01$ with $m_\pi = 139.57$ MeV the physical pion mass and $f_\pi = 92.3$ MeV the weak pion decay constant. Hence $t_{IJ}^{(n)}$ turns out to be proportional to λ^{2n} . In the $\pi\pi$ scattering case, the chiral expansion generates a hierarchy of corrections which depend on an increasing number of dimensionless and renormalization scale independent parameters. To lowest nontrivial order (LO, tree level) current algebra unique predictions for the scattering amplitudes $t_{IJ}^{(2)}(s)$ in terms of f_π and m_π are generated [11]. At next-to-leading order (NLO, one loop) four low energy parameters $\bar{T}_{1,2,3,4}$ determine the amplitude $t_{IJ}^{(4)}(s)$ [12,13]. At next-to-next-to-leading order (NNLO, two loops) the amplitude $t_{IJ}^{(6)}(s)$ can be expressed in terms of six parameters $\bar{b}_{1,2,3,4,5,6}$ [14,15]. Unlike the one-loop parameters $\bar{T}_{1,2,3,4}$, which can be fixed from ChPT calculations confronted with experimental data from several sources, the two-loop coefficients $\bar{b}_{1,2,3,4,5,6}$ are somewhat more difficult to fix directly from experiment since the amount of data close enough to threshold is scarce. Because of this problem and motivated by the success of the resonance saturation hypothesis at the one-loop level and at a renormalization scale $\mu = 750 \pm 250$ MeV [16], values for the

two-loop \bar{b} 's have been suggested on the basis of this hypothesis at that scale [15]. This causes the \bar{b} 's, independent in principle of the renormalization scheme, to have a spurious scale dependence. Since it is not really known what uncertainty should be assigned to this hypothesis, it has been suggested to ascribe a 100% error on the contributions to the low energy parameters determined by resonances [17].

The numerical consideration of errors from ChPT requires taking into account consistent sets of low energy parameters, both $\bar{T}_{1,2,3,4}$ and $\bar{b}_{1,2,3,4,5,6}$, deduced from several sources [18–22]. Moreover, there seem to be strong anticorrelations between \bar{T}_1 and \bar{T}_2 in the light of the two-loop K_{14} analysis [19,20]. This point has been thoroughly discussed in a previous work by two of us [23] and we refer the reader to it for further details. There, error propagation was undertaken in the form of a Monte Carlo simulation, instead of using parametric statistics, by generating a synthetic set of primary data. The basic assumption is that primary quantities, i.e., those obtained either directly from experiment or from an acceptable χ^2 fit, i.e., with a χ^2 per degree of freedom (DOF) ~ 1 , are Gauss distributed although perhaps with correlations. In practice, the distributions are represented by a population of finite but sufficiently large number ($N = 10^4$) of samples. The discussion in Ref. [23] amounts to having three compatible sets of one-loop \bar{T} and two-loop \bar{b} low energy parameter distributions deduced from several sources. They are summarized in Tables I and II. For consistency, we keep the same notation of our previous work. Set Ic in Ref. [23] corresponds to K_{14} decays, following the fits of Ref. [19] and some statistical modeling designed to reproduce the fragmentary information given in the K_{14} analysis of Ref. [19]. Set II corresponds to using D waves as proposed in the two-loop $\pi\pi$ scattering calculation in standard ChPT [15]. Finally, set III denotes the values of the low energy parameters obtained through Roy sum rules following the lines of Ref. [17]. We found in Ref. [23] that the anticorrelations between \bar{T}_1 and \bar{T}_2 persist in set III, although they are not very strong. In the present work we discard sets Ia and Ib as somewhat unrealistic. We also disregard set II because it produces too large errors as compared to sets Ic and III.

Despite its great success, ChPT does not incorporate exact unitarity to a given order of the expansion and hence cannot account for resonances, in particular for the ρ and σ reso-

*Email address: jmnieves@ugr.es

†Email address: earriola@ugr.es

¹We use the normalization such that the partial wave cross section is $\sigma_{IJ} = (2J+1)(4\pi/s)|t_{IJ}(s)|^2$. See also Eq. (2) below.

TABLE I. One-loop $\bar{T}_{1,2,3,4}$ low energy parameters in ChPT for the parameter sets Ic, II, and III of Ref. [23] as well as the correlation coefficient between \bar{T}_1 and \bar{T}_2 . In the present paper we use only Sets Ic and III.

Set	\bar{T}_1	\bar{T}_2	\bar{T}_3	\bar{T}_4	$r(\bar{T}_1, \bar{T}_2)$
Ic (K_{14} decays)	0.3 ± 1.2	4.77 ± 0.45	2.9 ± 2.4	4.4 ± 0.3	-0.69
II (D waves)	-0.8 ± 4.8	4.5 ± 1.1	2.9 ± 2.4	4.4 ± 0.3	-0.75
III (Roy sum rules)	-0.9 ± 1.2	4.34 ± 0.25	2.9 ± 2.4	4.4 ± 0.3	-0.22

nances which appear in the $I=1, J=1$ and $I=0, J=0$ channels, respectively. To deal with this problem, several unitarization methods have been devised in the past in the context of $\pi\pi$ scattering [24–36] (for a recent and short review, see, e.g., Ref. [37]). In those methods, unitarity is restored in the different partial wave amplitudes, while crossing is violated [30,34,40]. In the complex energy plane this corresponds to exactly taking into account the unitarity right hand elastic cut ($s > 4m_\pi^2$) but to approximating the left hand cut ($s < 0$). Detailed quantitative studies reveal that the approximation used to take into account the left hand cut does not become critical to describe phase shifts in the scattering region, but it may significantly influence the violation of crossing and the values of the low energy parameters. Thus, there is some confidence that unitarization methods can indeed be used to enlarge the domain of applicability of ChPT to the study of intermediate energy hadronic reactions. Among these unitarization approaches the inverse amplitude method (IAM) has been successfully applied to the description of meson-meson scattering, incorporating up to one-loop perturbative constraints. The original applications of the IAM involved dispersion relation arguments [27,29], which became rather cumbersome when incorporating coupled channels such as $K\bar{K}$ in $\pi\pi$ scattering. An algebraic derivation was soon found [32] to provide an almost trivial generalization to the coupled channel case, and a complete one-loop analysis for all meson-meson channels was carried out very recently in Ref. [33]. In addition to its very simple implementation from the standard chiral expansion, what makes this method particularly attractive is the fact that no new constants arise in

addition to those already present in standard ChPT. Furthermore, the IAM offers the possibility of systematic improvement according to the chiral expansion. Given the great success of this unitarization method in several meson-meson reactions including up to one-loop corrections, it seems almost obvious to extend the calculation to the (in principle) more accurate description up to two loops. As we will show below, such an extension is not as trivial as one might think. Actually, there was a previous calculation [31] where an analysis of the IAM for ChPT to two loops was undertaken. The conclusion was that the IAM is a well converged scheme. It is fair to say that no effort was made to assign uncertainties in the low energy parameters, making it somewhat hard to decide not only on the convergence itself but also on the compatibility with standard ChPT.

Recently, theoretical restrictions for the s -wave scattering lengths have been obtained from an analysis of Roy equations [41]. Unprecedented accuracy is obtained if, in addition to the relativistic, crossing, and unitarity demands from local quantum field theory, chiral symmetry constraints and the corresponding chiral expansion are implemented. The recent work [42] on matching the Roy equation analysis [41] to the two-loop ChPT expansion [14,15] has produced, using parametric statistics, the smallest error estimates for the low energy parameters so far. Roy equations provide an extremely elegant framework to incorporate crossing, analyticity, and unitarity constraints in $\pi\pi$ scattering amplitudes. The set of nonlinear inhomogeneous integral equations is not autonomous but requires some high energy tails obtained from experiment as input. In the low energy regime these so called driving terms can be described as polynomials, whose coefficients can be mapped to the low energy parameters of

TABLE II. Two-loop $\bar{b}_{1,2,3,4,5,6}$ low energy parameters in ChPT for the parameter sets Ic and III of Ref. [23] used in the present paper. The relation to the $b_{1,2,3,4,5,6}$ parameters used in this work is $\bar{b}_{1,2,3,4} = 16\pi^2 b_{1,2,3,4}$ and $\bar{b}_{5,6} = (16\pi^2)^2 b_{5,6}$. We also show explicitly the decomposition $\bar{b}_i = \bar{b}_i^0 + \Delta b_i$ referred to in Eq. (19).

Set	\bar{b}_1	\bar{b}_2	\bar{b}_3	\bar{b}_4	\bar{b}_5	\bar{b}_6
Ic	$-11.6_{-2.5}^{+2.4}$	11.2 ± 1.8	-0.2 ± 0.3	0.8 ± 0.1	$5.7_{-3.9}^{+3.2}$	$2.6_{-1.0}^{+0.8}$
III	$13.2_{-2.3}^{+2.5}$	$12.4_{-1.8}^{+1.7}$	$-0.4_{-0.2}^{+0.4}$	0.74 ± 0.06	$1.6_{-3.8}^{+3.7}$	$2.0_{-0.9}^{+0.8}$
Set	\bar{b}_1^0	\bar{b}_2^0	\bar{b}_3^0	\bar{b}_4^0	\bar{b}_5^0	\bar{b}_6^0
Ic	-9.1 ± 2	8.2 ± 1.7	0.3 ± 0.3	0.66 ± 0.07	$5.7_{-3.9}^{+3.2}$	$2.6_{-1.0}^{+0.8}$
III	$-10.7_{-2.0}^{+2.1}$	9.8 ± 1.7	-0.16 ± 0.40	0.58 ± 0.04	$1.6_{-3.8}^{+3.7}$	$2.0_{-0.9}^{+0.8}$
Set	$\Delta \bar{b}_1^0$	$\Delta \bar{b}_2^0$	$\Delta \bar{b}_3^0$	$\Delta \bar{b}_4^0$	$\Delta \bar{b}_5^0$	$\Delta \bar{b}_6^0$
Ic	$-2.4_{-0.4}^{+0.5}$	3.0 ± 0.3	$-0.5_{-0.1}^{+0.2}$	0.19 ± 0.04	0	0
III	$-2.4_{-0.4}^{+0.5}$	$2.6_{-0.3}^{+0.4}$	-0.4 ± 0.2	$0.15_{-0.04}^{+0.15}$	0	0

ChPT in the common region of validity of the Roy equations and ChPT. As a theoretical tool, the Roy equations cannot be solved by unitarization methods since the latter violate crossing to some extent. On the other hand, the Roy equations have not been generalized yet to other processes different from $\pi\pi$ scattering and require a knowledge of high energy data which may not always be available or accurate enough.² Taking this fact into account and the time elapsed since the original work [1] and the recent update [41], it would be desirable for Roy equation techniques to become a daily tool in hadronic physics, but it seems unlikely. In contrast, unitarization methods based on ChPT require in principle no more work than ChPT itself, which works well in the threshold region, but they are able to describe, in addition, resonance physics and have been successfully applied to a variety of problems. Because of this the unitarization of $\pi\pi$ scattering amplitudes using the IAM provides a model case where we can learn about the virtues and drawbacks of the method and also its convergence properties.

In the present work we study the IAM of unitarization of the two-loop ChPT amplitudes including a detailed error analysis based on the presently available information on the low energy parameters obtained from ChPT. By pursuing such a calculation we want to answer the question of whether or not low energy information plus unitarization reproduces the data beyond the domain of applicability of standard ChPT. In common with other unitarized calculations it is not clear how to avoid the unavoidable and prejudiced choice of a particular unitarization method. Moreover, given the unitarization method, it is hard to estimate uncertainties due to higher orders in the expansion. Our only hint so far is to compare successive orders in the scattering phase shifts with their corresponding error bars and determine whether or not practical convergence requirements are met. We do this analysis using sets Ic and III of one- and two-loop low energy parameters $\bar{l}_{1,2,3,4}$ and $\bar{b}_{1,2,3,4,5,6}$, respectively, of our previous work [23].

The paper is structured as follows. In Sec. II we provide some basic definitions in order to fix notation. We also estimate unitarity violations and the failure of a perturbative definition of phase shifts to describe the data in the region above threshold. In Sec. III we analyze the IAM phase-shift predictions as well as the corresponding threshold parameters, together with estimates of the amount of crossing violations in terms of Roskies sum rules [38,39], inherent to any unitarization method. Motivated by previous experiences, we believe that such crossing violations can be amended by a suitable generalization of the IAM. This point is analyzed in Sec. III E. Although there has been some work on the one-loop IAM of unitarization, we present in Sec. IV an updated analysis from the point of view of the convergence of the expansion for the unitarized phase shifts. Finally, we draw our main conclusions in Sec. V. In the Appendix we provide some information not presented in our previous paper [23]

²See, however, the recent work on πN scattering [43].

and also relevant for the present work, such as correlation matrices of both low energy constants and threshold parameters.

II. CHIRAL PERTURBATION THEORY TO TWO LOOPS AND UNITARITY VIOLATIONS

A. Basic definitions

Let $t_{IJ}(s)$ be the partial wave scattering amplitude for the reaction $\pi\pi \rightarrow \pi\pi$ at the center of mass (c.m.) energy \sqrt{s} in the IJ isospin-spin channel:

$$t_{IJ}(s) = \frac{e^{2i\delta_{IJ}(s)} - 1}{2i\sigma(s)} \quad (2)$$

with $\sigma(s) = \sqrt{1 - 4m_\pi^2/s}$ the c.m. momentum and $\delta_{IJ}(s)$ the corresponding phase shifts. Two-particle unitarity corresponds to real $\delta_{IJ}(s)$ and can be written as a nonlinear relation in the amplitude:

$$\text{Im } t_{IJ}(s) = \sigma(s) |t_{IJ}(s)|^2 \quad (3)$$

or, equivalently, as a linear relation in the inverse amplitude

$$\text{Im } t_{IJ}^{-1}(s) = -\sigma(s). \quad (4)$$

For a $\pi\pi$ scattering amplitude calculated in the chiral expansion sketched in Eq. (1), the lowest order amplitude $t_{IJ}^{(2)}(s)$ is a real function for S and P waves, and vanishes for D and higher waves. The NLO amplitude $t_{IJ}^{(4)}(s)$ develops an imaginary part for S and P waves but becomes real for D waves, and so on. The exact unitarity relation of Eq. (4) requires, at a perturbative level, the set of relations

$$\text{Im } t_{IJ}^{(2)}(s) = 0, \quad (5)$$

$$\text{Im } t_{IJ}^{(4)}(s) = \sigma(s) |t_{IJ}^{(2)}(s)|^2, \quad (6)$$

$$\text{Im } t_{IJ}^{(6)}(s) = 2\sigma(s) t_{IJ}^{(2)}(s) \text{Re } t_{IJ}^{(4)}(s). \quad (7)$$

Standard ChPT satisfies exact crossing symmetry at any order of the expansion, but violates unitarity. Two aspects are related to this violation. In the first place, a necessary condition for unitarity is the satisfaction of the inequality

$$\sigma(s) |t_{IJ}(s)| = |\sin \delta_{IJ}(s)| \leq 1. \quad (8)$$

This unitarity limit yields values of s slightly too high.³ A better way to quantify the unitarity violation is by defining the quantity

$$U_{IJ}(s) = |1 + 2i\sigma(s)t_{IJ}(s)|. \quad (9)$$

Below the two-pion production threshold $\sqrt{s} = 4m_\pi \sim 560$ MeV, the elastic unitarity condition requires $U_{IJ}(s)$

³For instance, for the isoscalar S wave one gets the inequality satisfied at LO in the range $s < 4\sqrt{\pi}f_\pi \sim 660$ MeV. We will show below that unitarity violations take place at significantly lower energies.

$=|e^{2i\delta_{IJ}(s)}|=1$. Strictly speaking, if unitarity is violated, $U_{IJ}(s) \neq 1$, there is no way other than perturbation theory for a real phase shift to satisfy simultaneously Eq. (1) and Eq. (2). Expanding Eq. (2) according to Eq. (1), the standard ChPT phase shift may be computed, yielding

$$\begin{aligned} \delta_{IJ}^{\text{ChPT}}(s) &= \frac{1}{2i} \ln[1 + 2i\sigma(s)t_{IJ}(s)] \\ &= \sigma(s)t_{IJ}^{(2)}(s) + \sigma(s)[t_{IJ}^{(4)}(s) - i\sigma(s)t_{IJ}^{(2)}(s)^2] \\ &\quad + \sigma(s)[t_{IJ}^{(6)}(s) - 2i\sigma(s)t_{IJ}^{(2)}(s)t_{IJ}^{(4)}(s) \\ &\quad - \frac{4}{3}\sigma(s)^2 t_{IJ}^{(2)}(s)^3] + \dots \end{aligned} \quad (10)$$

The elastic unitarity condition corresponds to $\delta_{IJ}^{\text{ChPT}}(s)$ being real, which is automatically satisfied if the perturbative unitarity relations, Eq. (7), are used, and one effectively gets

$$\begin{aligned} \delta_{IJ}^{\text{ChPT}}(s) &= \sigma(s)t_{IJ}^{(2)}(s) + \sigma(s)\text{Re} t_{IJ}^{(4)}(s) \\ &\quad + \sigma(s)[\text{Re} t_{IJ}^{(6)}(s) + \frac{2}{3}\sigma(s)^2 t_{IJ}^{(2)}(s)^3] + \dots \end{aligned} \quad (11)$$

Close to threshold, the scattering amplitude can be written in terms of the threshold parameters, scattering lengths a_{IJ} , and slopes b_{IJ} , defined by

$$t_{IJ}(s) = 2m_\pi(s/4 - m_\pi^2)^J [a_{IJ} + b_{IJ}(s/4 - m_\pi^2) + \dots]. \quad (12)$$

The scattering amplitudes $t_{IJ}(s)$ present kinematical zeros of order J at $s = 4m_\pi^2$. Chiral symmetry implies the existence of dynamical zeros for the S waves, named chiral or Adler zeros. In ChPT, Adler zeros may be determined perturbatively, i.e.,

$$t_{IJ}(s_A) = t_{IJ}^{(2)}(s_A) + t_{IJ}^{(4)}(s_A) + t_{IJ}^{(6)}(s_A) + \dots \quad (13)$$

Expanding the solution $s_A = s_A^{(2)} + s_A^{(4)} + s_A^{(6)} + \dots$, we get⁴

$$t_{IJ}^{(2)}(s_A^{(2)}) = 0, \quad (14)$$

$$s_A^{(4)} = -t_{IJ}^{(4)}(s_A^{(2)})/t_{IJ}^{(2)}(s_A^{(2)})', \quad (15)$$

$$\begin{aligned} s_A^{(6)} &= -t_{IJ}^{(6)}(s_A^{(2)})/t_{IJ}^{(2)}(s_A^{(2)})' \\ &\quad + \frac{t_{IJ}^{(4)}(s_A^{(2)})' t_{IJ}^{(4)}(s_A^{(2)})}{[t_{IJ}^{(2)}(s_A^{(2)})']^2}. \end{aligned} \quad (16)$$

At lowest order, nonkinematical zeros are located at

$$s_A^{(2)} = \frac{1}{2}m_\pi^2, \quad I=0, \quad J=0, \quad (17)$$

$$s_A^{(2)} = 2m_\pi^2, \quad I=2, \quad J=0. \quad (18)$$

⁴For a general function there would be a term involving the second derivative of $t_{IJ}^{(2)}$. This term disappears from the formulas since $t_{IJ}^{(2)}$ is a linear function of s .

From the formulas above, direct application of ChPT requires a scrupulous separation between different chiral orders. As we have already mentioned above, the NLO amplitudes $t_{IJ}^{(4)}(s)$ depend linearly on four dimensionless parameters $\bar{T}_{1,2,3,4}$. These parameters are supposed to be independent of f_π and m_π and therefore they are zeroth order in the chiral expansion.⁵ Finally, at NNLO the amplitude can be expressed in terms of six independent parameters $\bar{b}_{1,2,3,4,5,6}$. As was shown in the original two-loop calculation work [14,15] these \bar{b} coefficients contain a zeroth order piece and a second order piece:

$$\bar{b}_i = \bar{b}_i^0 + \Delta \bar{b}_i. \quad (19)$$

This makes the separation somewhat subtle because, when substituted into Eq. (1), an unwanted eighth order correction is induced. From the point of view of ChPT this contribution has to be dropped since the complete eighth order calculation is not available. On the other hand, these higher order corrections are numerically small as can be deduced from Table II.

B. Numerical results

The c.m. energy dependent figures with error bars presented in this work are generated as follows. If we have an energy dependent function F in terms of a set of random parameters (a_1, \dots, a_n) , distributed according to some statistical law, a random variable for any fixed value of s , $F(s; a_1, \dots, a_n)$ is generated. Obviously, for a nonlinear parameter dependent function the mean value of the curve is not equal to the function of the mean values, $\langle F(s; a_1, \dots, a_n) \rangle \neq F(s; \langle a_1 \rangle, \dots, \langle a_n \rangle)$. There is nothing wrong with this and one could simply bin the distributions for any fixed s value. Nevertheless, to make the results slightly more useful we wish to quote such a function of the mean values, $F(s; \langle a_1 \rangle, \dots, \langle a_n \rangle)$, as our central curves. To assign an upper and lower error bar (the distribution may in general be asymmetric) relative to this central value, we bin the distribution and first exclude the 16% top values and the 16% bottom values of the distribution. The remaining bins comprise 68% of the distribution values; the distances from the upper and lower values to our central value provide the upper and lower error bars, respectively. Evidently, our bands correspond to a 68% confidence level. This procedure of assigning errors fails for extremely asymmetric distributions, such that the central value turns out to be within the discarded upper or lower 16% intervals. Although we find that this situation seldom occurs in our calculation, in such a case we proceed in a different way. We first discard the 16% upper and lower intervals and then compute the arithmetic mean, which we assign as the central value. To control the quality of this second definition of central value, we compute

⁵Practical calculations require, however, a truncation of the chiral expansion and confrontation with experimental data, and hence some higher order systematic uncertainties remain in the one-loop parameters in addition to the experimental uncertainties.

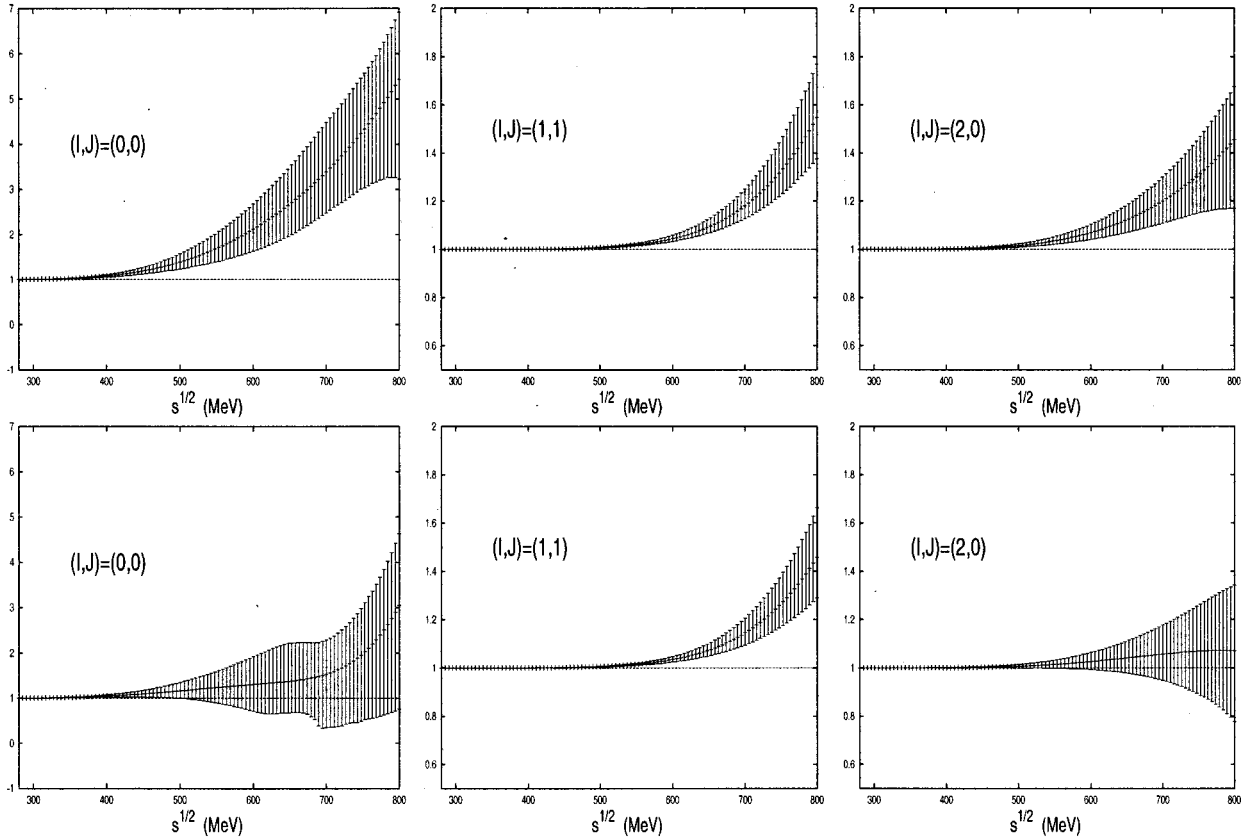


FIG. 1. Unitarity condition for standard NNLO ChPT amplitudes in $\pi\pi$ scattering for S and P waves defined by $U_{IJ}(s) = |1 + 2i\sigma(s)t_{IJ}(s)|$. Upper panels: Set Ic of Ref. [23]. Lower panels: Set III of Ref. [23]. In the calculation the parameters \bar{b}_i^0 defined in Eq. (19) and given in Table II have been used. The unitarity condition requires $U_{IJ}(s) = 1$.

both definitions whenever possible, and find that the differences are numerically less significant than the error bars.

The results for the unitarity condition $U_{IJ}(s)$ as defined in Eq. (9), can be seen in Figs. 1 and 2 in terms of the \bar{b}_i^0 and $\bar{b}_i = \bar{b}_i^0 + \Delta\bar{b}_i$ coefficients, respectively, and for the parameter sets Ic and III. As we see, standard ChPT violates unitarity in a systematic manner well below the resonance region including uncertainties for set Ic. For set III only the P wave exhibits this behavior, due to large uncertainties in the S -wave unitarity violation. The perturbatively defined phase shifts, $\delta_{IJ}^{\text{ChPT}}(s)$ as given by Eq. (10) can be seen in Figs. 3 and 4 in terms of the \bar{b}_i^0 and $\bar{b}_i = \bar{b}_i^0 + \Delta\bar{b}_i$ coefficients, respectively, and for the parameter sets Ic and III. As we see from the figures, the perturbatively defined phase shifts seem compatible with experimental data whenever the corresponding unitarity condition is compatible within uncertainties with elastic unitarity. Let us recall that threshold parameters for set III have uncertainties similar to or slightly smaller than set Ic [23]. This also holds for higher energies but there appear some systematic discrepancies with the data, slightly favoring Set III.

Threshold parameters for sets Ic and III at the two-loop level were computed in our previous work [23]. There, a separation of the tree-level, one-loop, and two-loop contributions with their corresponding error estimates was presented.

The partial S - and P -wave amplitudes in the unphysical region below threshold and above the left cut, $0 \leq 0 \leq 4m_\pi^2$, are depicted in Fig. 5. In this region partial wave amplitudes are real and present real single zeros. The single zero at $4m_\pi^2$ in the P wave is of kinematical origin as can be seen from Eq. (12). However, zeros in the S waves are dynamical consequences of chiral symmetry. As we see, the agreement between the parameter sets Ic and III is very good within uncertainties. The two-loop location of Adler zeros with error estimates is given in Table III. The additive structure of the ChPT amplitude makes a numerically small distinction in the separation $\bar{b}_i = \bar{b}_i^0 + \Delta\bar{b}_i$. As we see, the isotensor S -wave chiral zero does not move within uncertainties from its tree-

TABLE III. Nonkinematical Adler zeros for S -wave $I=0$ and 2 amplitudes for ChPT and the parameter sets Ic and III of Ref. [23]. We also indicate the phase-shift figures that correspond to these zeros. Errors are given in parentheses.

s_A/m_π^2	$(I,J)=(0,0)$	$(I,J)=(2,0)$
ChPT Ic Fig. 2	0.38(6)	2.03(5)
ChPT III Fig. 2	0.43(6)	2.00(5)
ChPT' Ic Fig. 4	0.38(6)	2.03(5)
ChPT' III Fig. 4	0.43(6)	2.00(5)

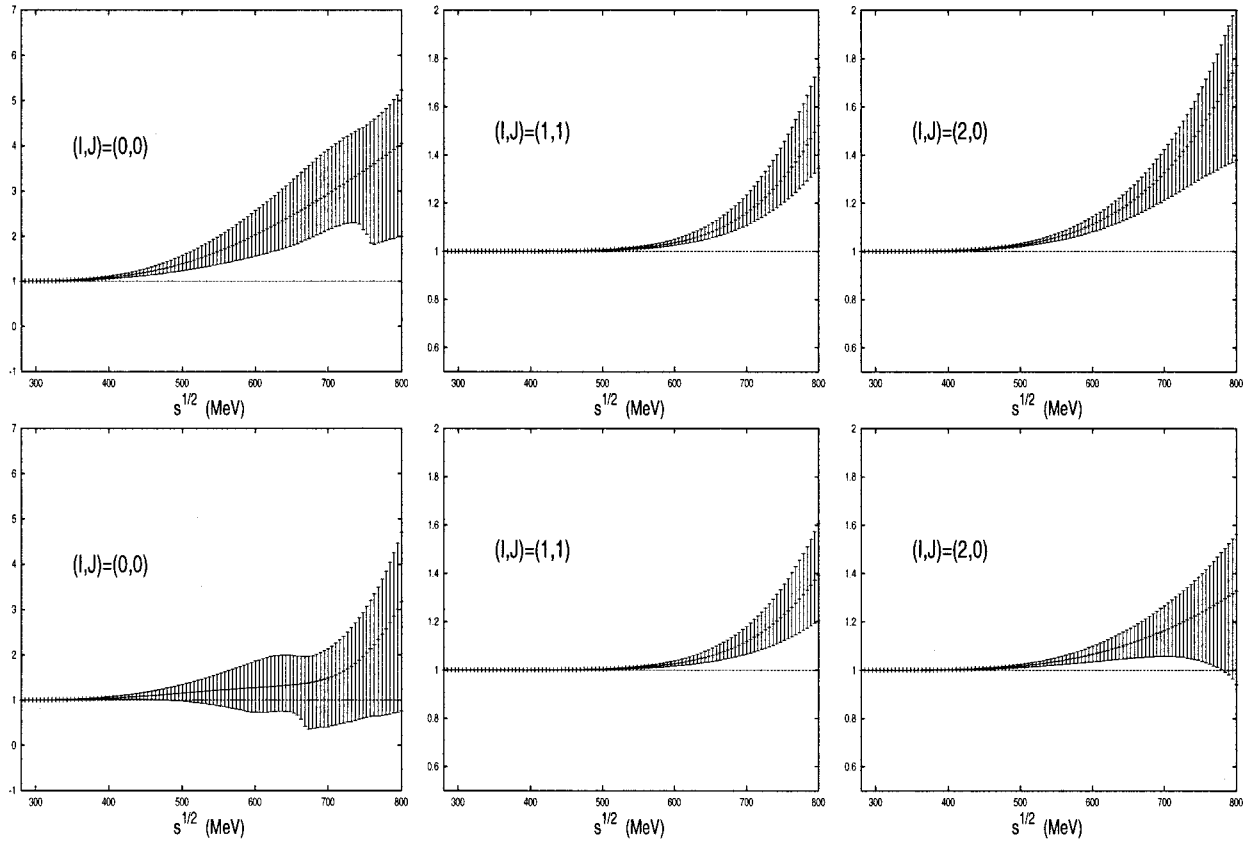


FIG. 2. Unitarity condition for standard NNLO ChPT amplitudes in $\pi\pi$ scattering for S and P waves defined by $U_{IJ}(s) = |1 + 2i\sigma(s)t_{IJ}(s)|$. Upper panels: Set Ic of Ref. [23]. Lower panels: Set III of Ref. [23]. In the calculation the parameters \bar{b}_i defined in Eq. (19) and given in Table II have been used. The unitarity condition requires $U_{IJ}(s) = 1$.

level value of Eq. (18) for either set Ic, or set III. For the parameter set III, the two-loop shift of the S -wave isoscalar Adler zero also almost does not move. Nevertheless, for parameter set Ic there is a systematic shift of about 20%.

III. INVERSE AMPLITUDE METHOD TO TWO LOOPS AND PERTURBATIVE MATCHING

A. Algebraic derivation

The idea of the method is quite simple and we review it here for the sake of completeness. If, instead of expanding the amplitude, one considers the inverse amplitude and expands according to the chiral expansion [assuming $t_{IJ}^{(2)}(s) \neq 0$], one gets

$$\begin{aligned} \frac{1}{t_{IJ}(s)} &= \sigma(s) \cot \delta_{IJ}^{\text{IAM}}(s) - i\sigma(s) \\ &= \frac{1}{t_{IJ}^{(2)}(s)} - \frac{t_{IJ}^{(4)}(s)}{t_{IJ}^{(2)}(s)^2} + \left[\frac{t_{IJ}^{(4)}(s)^2}{t_{IJ}^{(2)}(s)^3} - \frac{t_{IJ}^{(6)}(s)}{t_{IJ}^{(2)}(s)^2} \right] + \dots \end{aligned} \quad (20)$$

One may check that the unitarity relation Eq. (4) is exactly preserved because of the perturbative relations of Eq. (7). Note that a direct application of the IAM including up to two loops can unitarize only S and P waves. To unitarize D

waves a three-loop calculation would be needed. Since such a calculation has not yet been done, we will restrict ourselves to S and P waves in the present work. The structure of Eq. (20) makes it possible to have poles in the second Riemann sheet, i.e., zeros of $t^{-1}(s)$, but this is done at the expense of some fine-tuning between several orders. Actually, the IAM assumes that the inverse amplitude $1/t_{IJ}(s)$ is small, which is particularly true in the neighborhood of a resonance.

B. Inverse amplitude method phase shifts

The best way to quantify the goodness of a unitarization scheme such as the IAM is to check whether or not the information contained in the low energy parameters, in conjunction with the unitarized amplitude given by Eq. (20), predicts within acceptable errors the phase shifts in the region above the threshold. To proceed further we have to fix in some way our sets of parameters. An alternative, and actually complementary, point of view is to make a direct fit to the data. Unfortunately, this involves a ten-parameter fit, and moreover there are some parameters, like for instance \bar{L}_3 and \bar{L}_4 , for which $\pi\pi$ scattering is not very sensitive. Actually, as was recognized in Ref. [42], there are two kinds of low energy parameters according to the properties of the corresponding terms in the partial wave amplitudes: Class A, terms that survive in the chiral limit, comprising \bar{L}_1 , \bar{L}_2 , r_5 , and r_6 ;

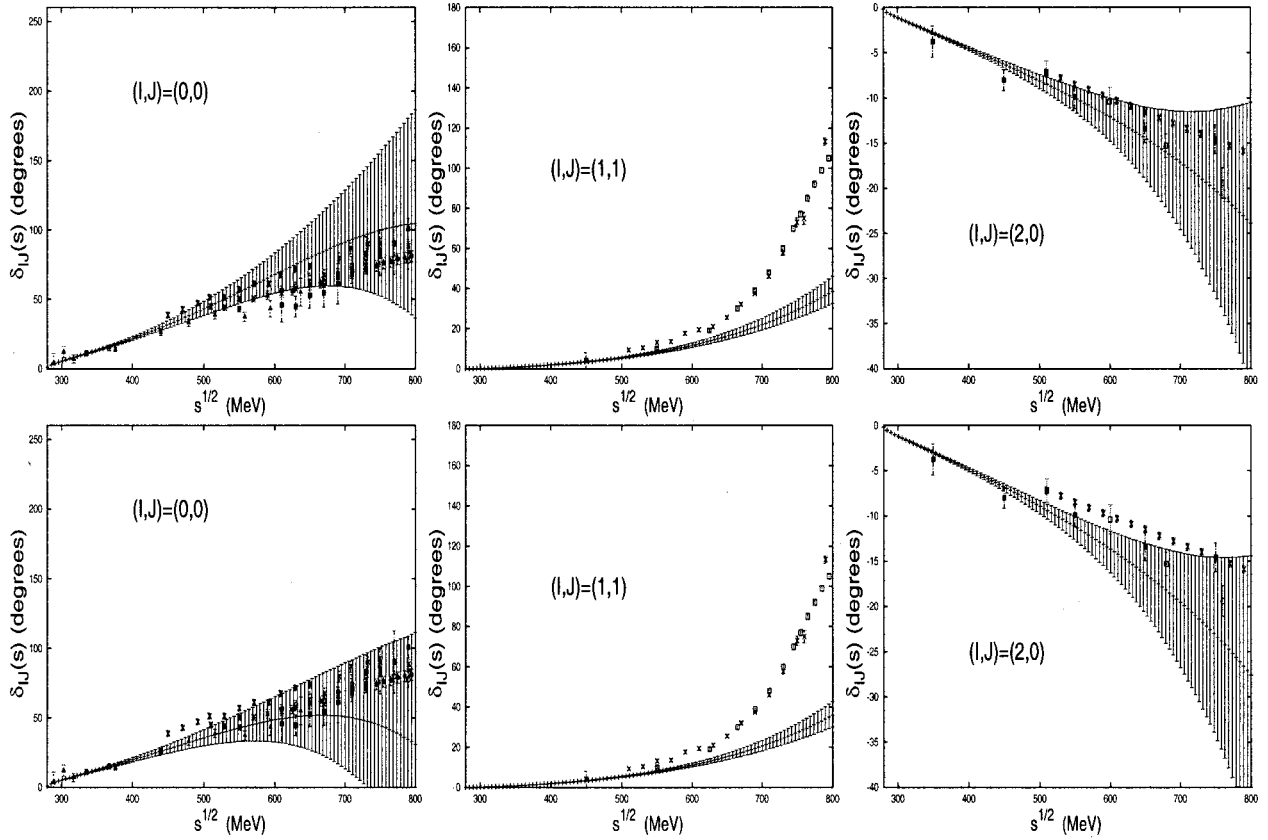


FIG. 3. Standard NNLO ChPT phase shifts (in degrees) for $\pi\pi$ scattering for S and P waves after Eq. (10). Upper panels: Set Ic of Ref. [23]. Lower panels: Set III of Ref. [23]. In the calculation the parameters \bar{b}_i^0 defined in Eq. (19) and given in Table II have been used. Combined data from Refs. [2–10].

and class B, symmetry breaking terms corresponding to the remaining low energy parameters \bar{l}_3 , \bar{l}_4 , r_1 , r_2 , r_3 , and r_4 . The r_i parameters determine the pure two-loop contribution to the amplitude. On the basis that chiral symmetry breaking is a small effect, we expect a higher sensitivity of the scattering data to variations of the class A parameters.

1. Naive scheme

The simplest and most direct way to look at the quantitative predictions of the IAM is to take the unitarized amplitude Eq. (20) for all partial waves and propagate the errors in the one- and two-loop parameters $\bar{l}_{1,2,3,4}$ and $\bar{b}_{1,2,3,4,5,6}$, respectively. As we have already pointed out, this may be a dangerous procedure since the two-loop parameters contain a higher order piece, but one might argue that, since the numerical effect on the \bar{b} 's should be small (see Table II), one might expect an overall small effect anyhow. Along these lines, we present in Fig. 6 the results obtained by using the parameter sets Ic and III of Ref. [23]. As can be seen from the figures, the errors are huge and there is even a trend to discrepancy in the ρ channel for set III.

2. Monte Carlo scheme

Having realized the dangers of making a naive Monte Carlo error propagation from the analysis of Ref. [23], we

proceed now in a different manner. We consider sets Ic and III of Ref. [23] for both the one-loop \bar{l}_i parameters and the zeroth order two-loop parameters \bar{b}_i^0 as explicitly given in the Appendix of Ref. [15]. The results are shown in Fig. 7. Although in the S waves there are no big differences as compared to Fig. 6, in the ρ channel the effect at intermediate energies not only makes the predicted phase shifts compatible with data but also the error bars are substantially reduced.

3. Partial fit scheme

The results of the two previous schemes suggest that some fine-tuning mechanism is needed, since the large difference between them is due to either considering the \bar{b} parameters as a whole or explicitly splitting them as different orders, according to $\bar{b}_i = \bar{b}_i^0 + \Delta\bar{b}_i$. This fact seems to indicate that their numerical values may be constrained to a large extent by performing a χ^2 fit. As we have mentioned above this involves ten parameters. Another possibility might be to make selective fits in some subsets of parameters and propagate the errors in the remaining ones. After trying out several combinations, we have found that, indeed, the low energy parameters of class A, i.e., those not vanishing in the chiral limit, are enough for a satisfactory fit to the data. In practice, the procedure is as follows. For either set Ic or set III, we

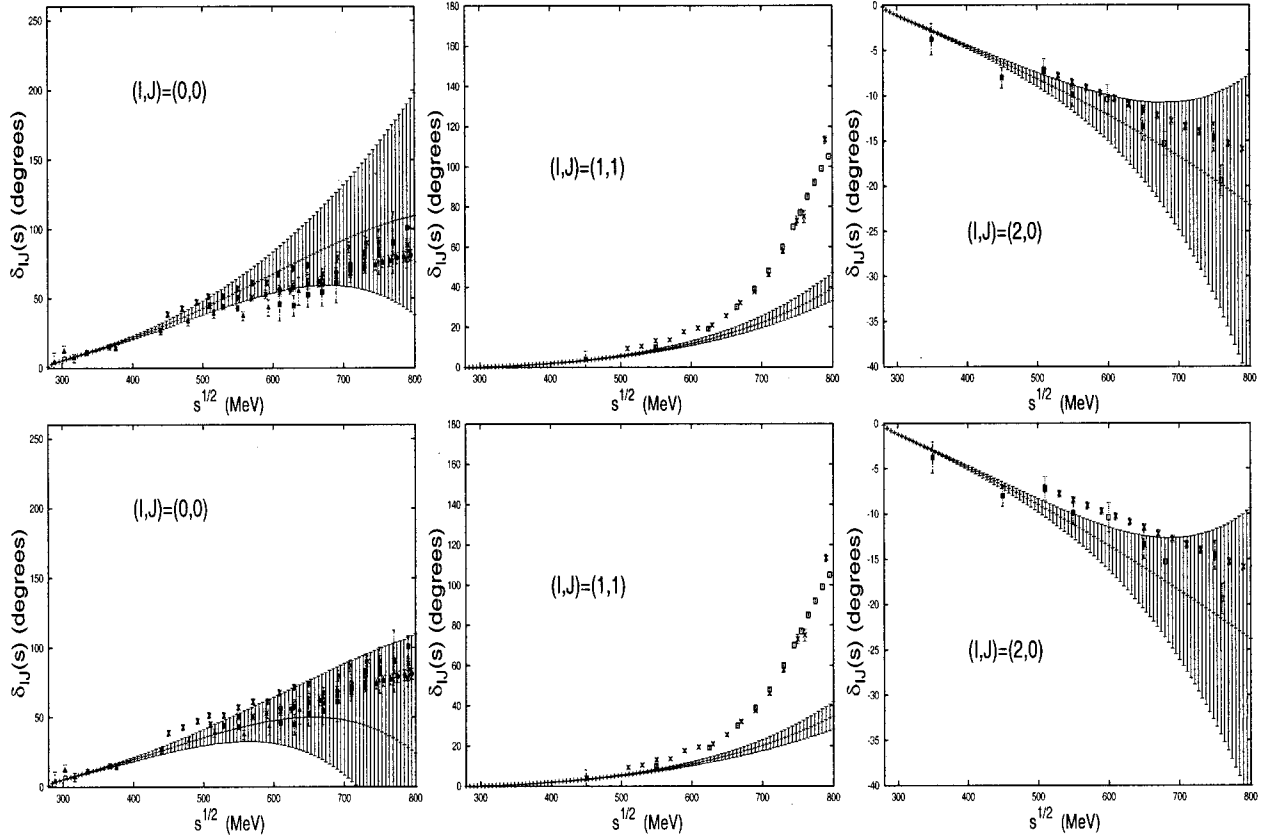


FIG. 4. Standard NNLO ChPT phase shifts (in degrees) for $\pi\pi$ scattering for S and P waves after Eq. (10). Upper panels: Set Ic of Ref. [23]. Lower panels: Set III of Ref. [23]. In the calculation the parameters \bar{b}_i defined in Eq. (19) and given in Table II have been used. Combined data from Refs. [2–10].

generate a sufficiently large sample ($N=10^4$ proves large enough) of class B parameters, i.e., those corresponding to chiral symmetry breaking terms in the $\pi\pi$ scattering amplitudes. For any member of the class B parameter population a χ^2 fit of class A parameters is performed. This procedure yields distributions for \bar{l}_1 , \bar{l}_2 , r_5 , and r_6 parameters, whence straightforward error analysis may be undertaken. The choice of these parameters rather than the \bar{b} 's has the advantage that the separation $\bar{b}_i = \bar{b}_i^0 + \Delta\bar{b}_i$ may be explicitly done within the fitting procedure, and hence a correct book-keeping of chiral orders in the inverse amplitude is implemented. The result of the fit is⁶

$$\begin{aligned} \bar{l}_1 &= -0.14_{-0.74}^{+0.62}, & \bar{l}_2 &= 4.4 \pm 0.1, \\ 10^4 r_5 &= 1.07_{-0.35}^{+0.31}, & 10^4 r_6 &= -0.35_{-0.34}^{+0.13}, \end{aligned} \quad (21)$$

which produces χ^2 / DOF of $69.9/(67-4)=1.11$, a rather satisfactory value as can also be clearly seen in Fig. 8. In

⁶We apply the following energy cuts and scattering data. For the isoscalar S wave we cut at $\sqrt{s}=610$ MeV the data of Refs. [2–4,6–8]. For the isotensor S wave we cut at 970 MeV the data of Refs. [9,5]. For the isovector P wave we cut at 1 GeV.

addition, we obtain the correlation coefficient $r(\bar{l}_1, \bar{l}_2) = 0.22$. There are no set Ic and set III labels because \bar{l}_1 and \bar{l}_2 , which provide this label, are determined from the fit. Both class A and class B parameters contribute to the total errors. The errors corresponding to fitted (class A) low energy parameters can be determined by employing the standard procedure of changing the χ^2 from its minimal value by one unit. We find that they are rather small, so the quoted errors in Eq. (21) are dominated by the uncertainties in the class B low energy parameters and the scale at which resonance saturation is assumed, $\mu = 750 \pm 250$ MeV.

As we see, the resulting values of the fitted parameters, particularly \bar{l}_1 and \bar{l}_2 , are very much in agreement with the standard ChPT estimates of Ref. [23]. It is also interesting to note that the values of r_5 and r_6 are consistent within error bars with those assumed from resonance saturation provided with 100% uncertainty as suggested in Ref. [17]. Transforming these values into \bar{b} parameters, we get

$$\begin{aligned} \bar{b}_1 &= -12.1_{-2.2}^{+1.9}, & \bar{b}_2 &= 11.5_{-1.0}^{+1.2}, & \bar{b}_3 &= -0.29_{-0.27}^{+0.20}, \\ \bar{b}_4 &= 0.75 \pm 0.02, & \bar{b}_5 &= 3.14_{-0.56}^{+0.42}, & \bar{b}_6 &= 0.55_{-0.64}^{+0.46}. \end{aligned} \quad (22)$$

These numbers have been constructed by adding the resulting \bar{b}_i^0 to the second order $\Delta\bar{b}_i$ contribution, although both

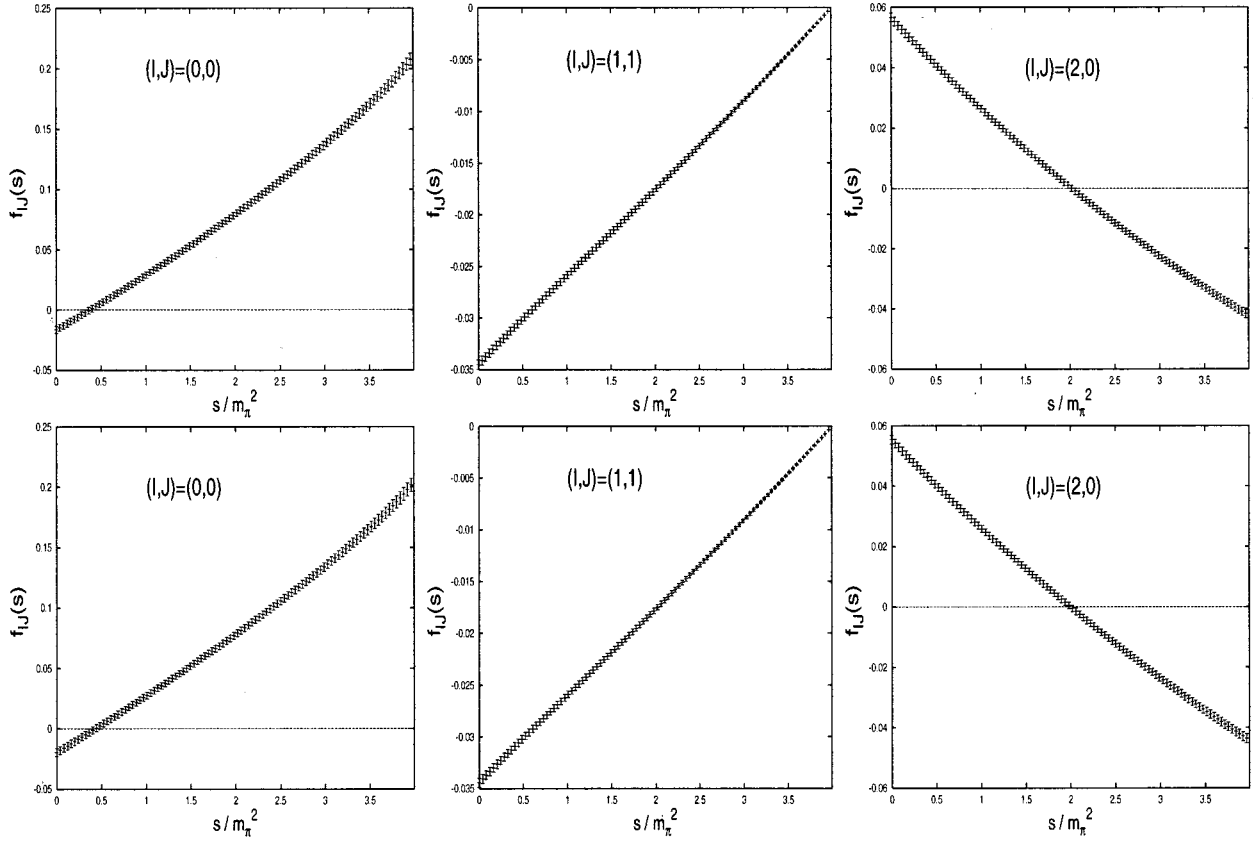


FIG. 5. S and P partial wave amplitudes $f_{IJ}(s) = \sqrt{s}t_{IJ}(s)$ (in fm) for $\pi\pi$ scattering in standard ChPT to two loops in the unphysical region $0 \leq s \leq 4m_\pi^2$. Upper panels: Set Ic of Ref. [23]. Lower panels: Set III of Ref. [23]. Normalization is such that at $s = 4m_\pi^2$ one has the scattering length for the S waves. In the scattering region ($s > 4m_\pi^2$) this figure corresponds to Fig. 3.

contributions enter the fit in a nonadditive way. As we see, the resulting values agree with those expected from standard ChPT analyses within uncertainties, with the sole exception of \bar{b}_6 , which turns out to be inconsistent. The reason is that the corresponding value for r_6 comes out with exactly opposite sign to that expected in resonance saturation.

Finally, we present in Fig. 9 the IAM unitarized partial S - and P -wave amplitudes in the unphysical region $0 \leq s \leq 4m_\pi^2$ using the Monte Carlo scheme for both sets Ic and III. Obviously, the kinematical zero of the P wave at $s = 4m_\pi^2$ remains fixed. On the other hand, the nonkinematical Adler zeros of the S -wave amplitudes do not move from their lowest order locations given by Eq. (18) but become higher order zeros, as can be observed from the figures in the small bumps around the zeros, and analytically in Eq. (20). Although this effect is undesirable, we see that from a direct comparison of the standard ChPT amplitudes of Fig. 5 with the IAM unitarized ones of Fig. 9 one may conclude that the violation of the order of the nonkinematical zero does not have dramatic quantitative consequences.

C. Crossing violations

As we have said, the IAM restores unitarity but violates crossing symmetry. The interesting point is that although unitarization, which has to do with the right hand cut, may provide a satisfactory energy dependence and hence a de-

scription of the data in the scattering region, it can still do so with low energy constants (LEC's) that differ from those expected in standard ChPT. The precise numerical values of the LEC's depend on how the left hand cut is handled and approximated before and after unitarization. On the other hand, a proper left hand cut is a direct consequence of crossing symmetry in the s, t, u representation. It is therefore interesting to study these crossing violations on a quantitative basis. A particular way of doing this at the level of partial wave amplitudes is by using Roskies sum rules [38,39]. Two methods at least have been introduced in the literature to characterize crossing violations in a quantitative way. Defining the quantities introduced in Ref. [30],

$$C_1 = \int_0^{4m_\pi^2} ds (4m_\pi^2 - s)(3s - 4m_\pi^2)[t_{00}(s) + 2t_{20}(s)], \quad (23)$$

$$C_2 = \int_0^{4m_\pi^2} ds (4m_\pi^2 - s)[2t_{00}(s) - 5t_{20}(s)],$$

$$C_3 = \int_0^{4m_\pi^2} ds \{ (4m_\pi^2 - s)(3s - 4m_\pi^2)[2t_{00}(s) - 5t_{20}(s)] + 9(4m_\pi^2 - s)^2 t_{11}(s) \},$$

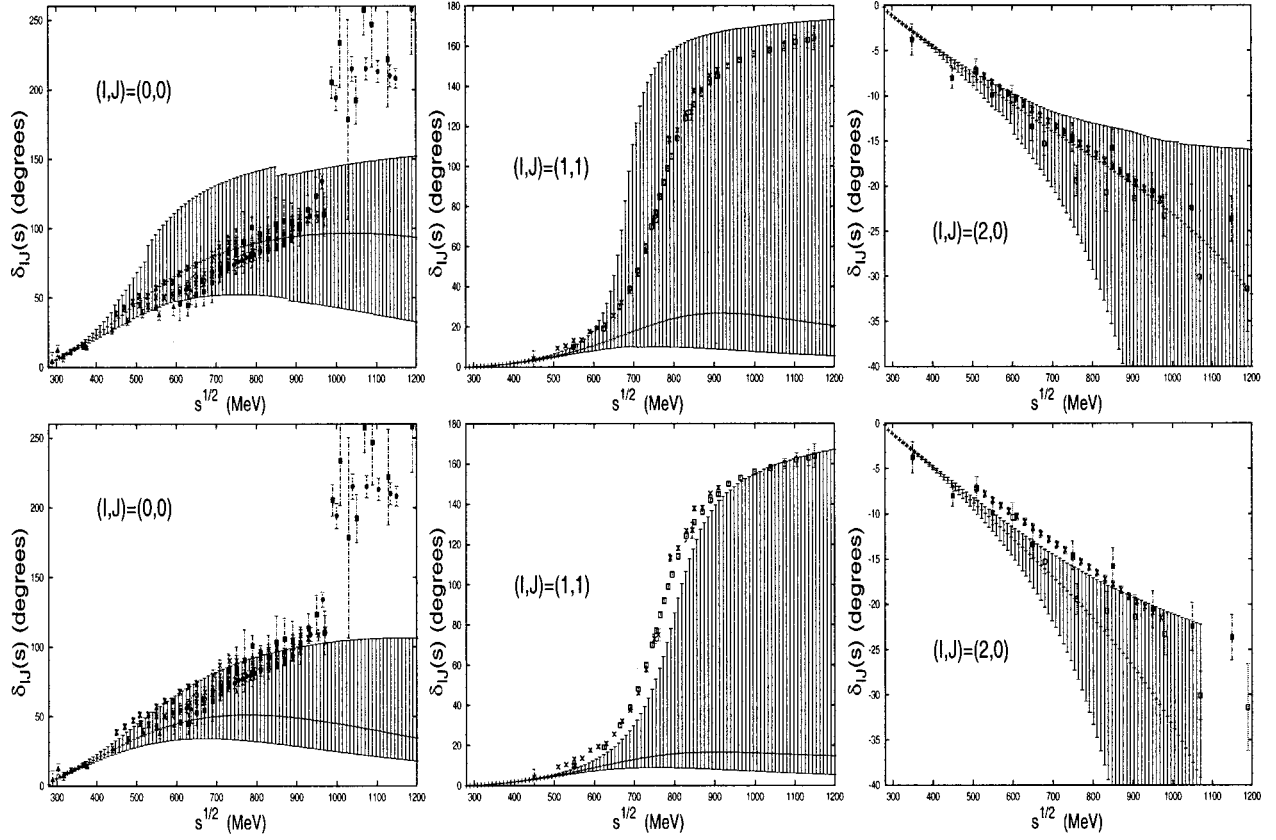


FIG. 6. IAM unitarized phase shifts (in degrees) for $\pi\pi$ scattering for S and P waves. Naive scheme (see main text). Upper panels: Set Ic of Ref. [23]. Lower panels: Set III of Ref. [23]. Combined data from Refs. [2–10].

$$\begin{aligned}
 C_4 &= \int_0^{4m_\pi^2} ds \{ (4m_\pi^2 - s)s^2 [2t_{00}(s) - 5t_{20}(s)] \\
 &\quad + 3(4m_\pi^2 - s)^3 t_{11}(s) \}, \\
 C_5 &= \int_0^{4m_\pi^2} ds \{ (4m_\pi^2 - s)^2 s^2 [2t_{00}(s) - 5t_{20}(s)] \\
 &\quad + 3(4m_\pi^2 - s)^2 (8m_\pi^2 - 3s) s t_{11}(s) \}.
 \end{aligned}$$

These relations can be written in the general form

$$C_i = \int_0^{4m_\pi^2} ds \sum_{IJ} \omega_{IJ,i}(s) t_{IJ}(s). \quad (24)$$

Crossing symmetry implies $C_i = 0$. We also consider the definitions introduced in Ref. [40]:

$$\begin{aligned}
 A_1 &= 2 \int_0^{4m_\pi^2} ds (s - 4m_\pi^2) t_{00}(s), \\
 B_1 &= 5 \int_0^{4m_\pi^2} ds (s - 4m_\pi^2) t_{20}(s), \\
 A_2 &= \int_0^{4m_\pi^2} ds (s - 4m_\pi^2) (3s - 4m_\pi^2) t_{00}(s),
 \end{aligned} \quad (25)$$

$$B_2 = -2 \int_0^{4m_\pi^2} ds (s - 4m_\pi^2) (3s - 4m_\pi^2) t_{20}(s),$$

$$A_3 = \int_0^{4m_\pi^2} ds (s - 4m_\pi^2) (3s - 4m_\pi^2) t_{00}(s),$$

$$B_3 = 2 \int_0^{4m_\pi^2} ds (s - 4m_\pi^2)^2 t_{11}(s),$$

$$A_4 = \int_0^{4m_\pi^2} ds (s - 4m_\pi^2) (3s - 4m_\pi^2) \{ 2t_{00}(s) - 5t_{20}(s) \},$$

$$B_4 = 9 \int_0^{4m_\pi^2} ds (s - 4m_\pi^2)^2 t_{11}(s),$$

$$\begin{aligned}
 A_5 &= \int_0^{4m_\pi^2} ds (s - 4m_\pi^2) (10s^2 - 32sm_\pi^2 + 16m_\pi^4) \\
 &\quad \times \{ 2t_{00}(s) - 5t_{20}(s) \},
 \end{aligned}$$

$$B_5 = -6 \int_0^{4m_\pi^2} ds (s - 4m_\pi^2)^2 (5s - 4m_\pi^2) t_{11}(s),$$

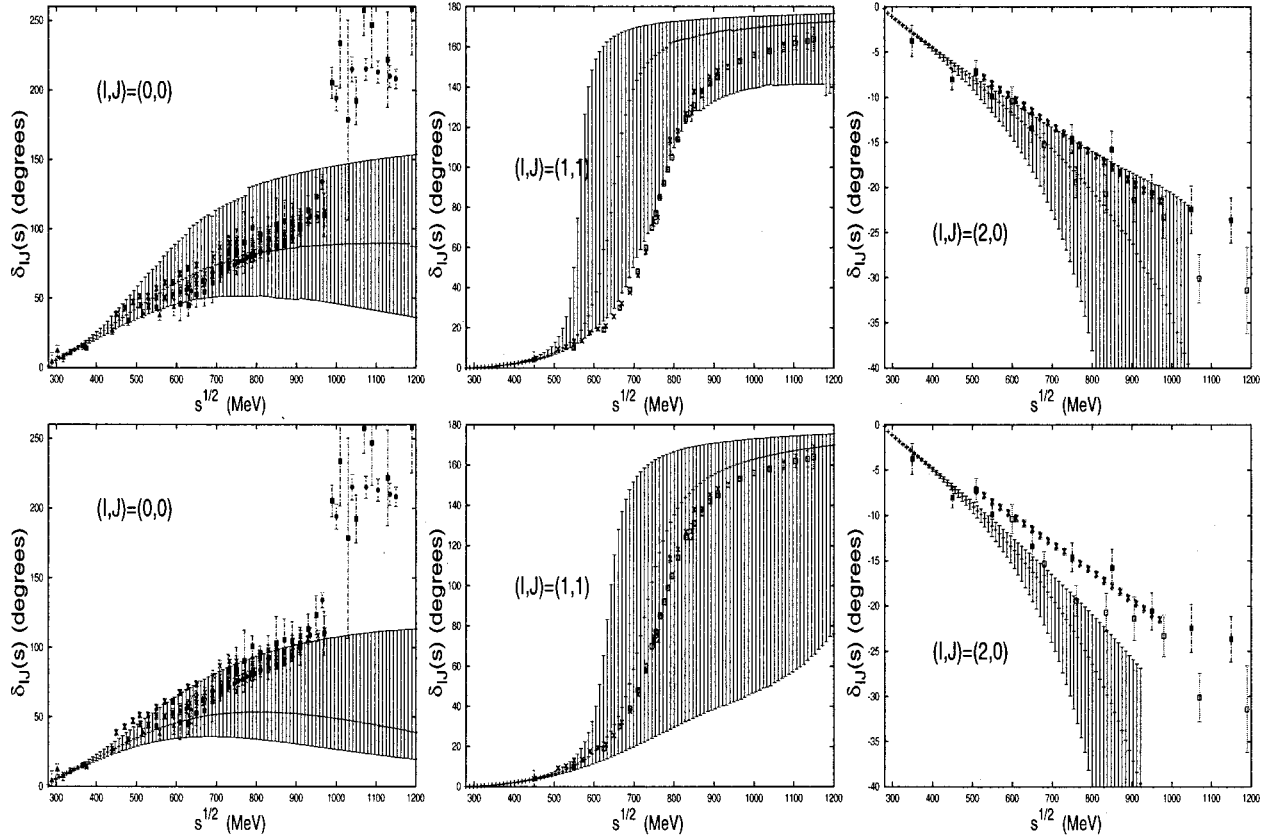


FIG. 7. IAM unitarized phase shifts (in degrees) for $\pi\pi$ scattering for S and P waves. Monte Carlo scheme (see main text). Upper panels: Set Ic of Ref. [23]. Lower panels: Set III of Ref. [23]. Combined data from Refs. [2–10].

$$A_6 = \int_0^{4m_\pi^2} ds (s - 4m_\pi^2) (35s^3 - 180s^2m_\pi^2 + 240sm_\pi^4 - 64m_\pi^6) \\ \times \{2t_{00}(s) - 5t_{20}\},$$

$$B_6 = 15 \int_0^{4m_\pi^2} ds (s - 4m_\pi^2)^2 (21s^2 - 48sm_\pi^2 + 16m_\pi^4) t_{11}(s).$$

Crossing symmetry implies in this case $A_i - B_i = 0$ for i from 1 to 6. Formally, if the unitarized amplitudes embody ChPT to some order, these sum rules will be identically verified to the same order. In previous work, the numerical satisfaction of the sum rules has been tested to one and two loops, but no error estimates have been taken into account. Because of this, some *ad hoc* dimensionless crossing violations have been defined [30,40]. In Refs. [30,34] the ratio

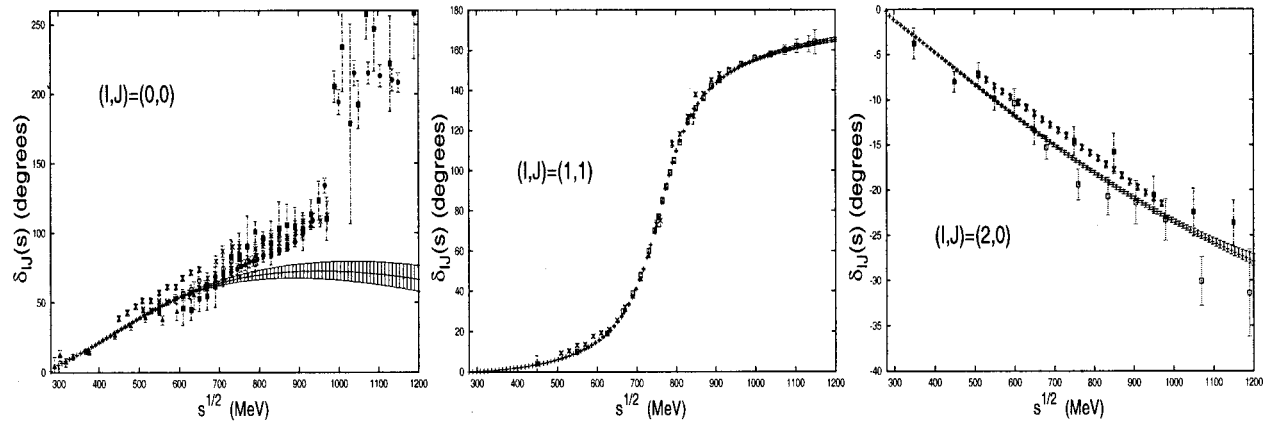


FIG. 8. IAM unitarized phase shifts (in degrees) for $\pi\pi$ scattering for S and P waves. Partial fit scheme (see main text). There are no set Ic and set III labels because \bar{I}_1 and \bar{I}_2 , which provide this label, are determined from the fit. Combined data from Refs. [2–9]. Uncertainties in the curves stem from those of class B parameters and the scale for which resonance saturation is assumed, $\mu = 750 \pm 250$ MeV.

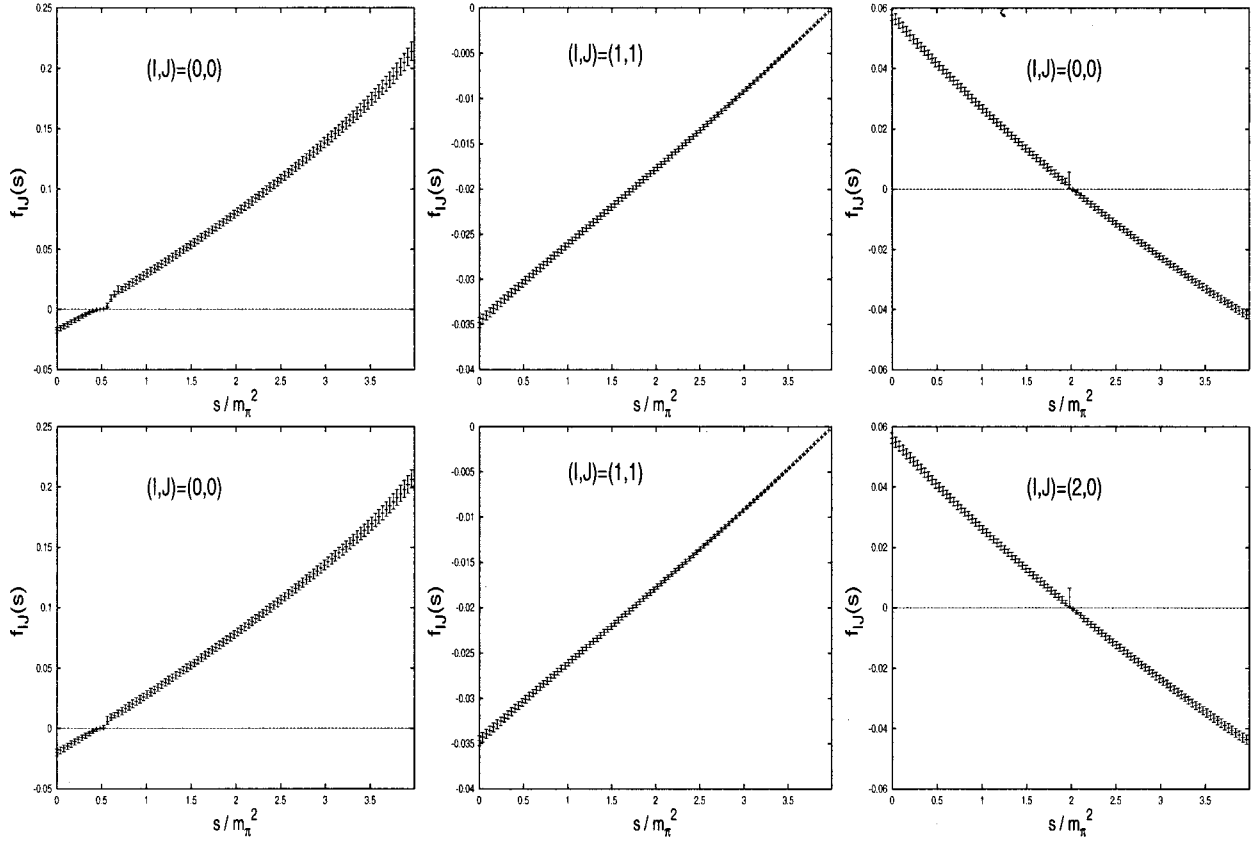


FIG. 9. S and P partial wave amplitudes $f_{lJ}(s) = \sqrt{s}t_{lJ}(s)$ (in fm) for $\pi\pi$ scattering in the IAM to two loops in the unphysical region $0 \leq s \leq 4m_\pi^2$. Monte Carlo scheme. Upper panels: Set Ic of Ref. [23]. Lower panels: Set III of Ref. [23]. Normalization is such that at $s = 4m_\pi^2$ one has the scattering length for the S waves. In the scattering region ($s > 4m_\pi^2$) this figure corresponds to Fig. 7.

$$R_i = 100 \times \frac{\int_0^{4m_\pi^2} ds \sum_{IJ} \omega_{IJ,i}(s) t_{IJ}(s)}{\int_0^{4m_\pi^2} ds \left| \sum_{IJ} \omega_{IJ,i}(s) t_{IJ}(s) \right|} \quad (26)$$

$$V_i = 100 \times \left| \frac{A_i - B_i}{A_i + B_i} \right| \quad (27)$$

is introduced,⁷ whereas in Ref. [40] the violation

is defined. The advantage of providing error bars to the crossing sum rules $C_i = 0$ or $A_i - B_i = 0$ is obvious; the dimensionless quantity is naturally defined as the size of the uncertainty relative to the mean value. This allows one to make a definite statement on crossing violations in terms of

TABLE IV. Roskies sum rule violations in percentages as defined by Eq. (27) and introduced in Ref. [40] for the IAM method and the parameter sets Ic and III of Ref. [23]. We also indicate the phase-shift figures that generate these violations

IAM	V_1	V_2	V_3	V_4	V_5	V_6
Set Ic naive. Figure 6	$0.9^{+0.6}_{-0.7}$	$0.9^{+0.7}_{-0.5}$	$0.9^{+0.8}_{-0.5}$	$0.4^{+0.4}_{-0.3}$	33^{+62}_{-21}	6^{+13}_{-67}
Set III naive. Figure 6	$0.3^{+0.2}_{-0.6}$	$0.4^{+0.6}_{-0.2}$	$0.4^{+0.6}_{-0.3}$	$0.15^{+0.17}_{-0.30}$	14^{+40}_{-13}	2^{+22}_{-61}
Set Ic non-naive Figure 7	$0.7^{+0.4}_{-0.6}$	$0.7^{+0.6}_{-0.5}$	$0.9^{+0.8}_{-0.6}$	$0.5^{+0.5}_{-0.4}$	22^{+29}_{-19}	4^{+12}_{-14}
Set III non-naive. Figure 7	$0.3^{+0.5}_{-0.1}$	$0.3^{+0.5}_{-0.2}$	$0.4^{+0.6}_{-0.3}$	$0.2^{+0.4}_{-0.2}$	9^{+23}_{-15}	6^{+10}_{-15}
Fit of Figure 8	$0.5^{+0.5}_{-0.3}$	$0.5^{+0.5}_{-0.3}$	$0.5^{+0.6}_{-0.4}$	$0.3^{+0.3}_{-0.3}$	12^{+19}_{-25}	7^{+21}_{-7}

⁷We use specifically the formula proposed in Ref. [34] since it is unambiguous. The formula of Ref. [30] is misleading, probably due to a misprint.

TABLE V. Sum rule violations in percentages as defined by Eq. (26) and introduced in Refs. [30,34] for the IAM and the parameter sets Ic and III of Ref. [23]. We also indicate the phase-shift figures that generate these violations

IAM	R_1	R_2	R_3	R_4	R_5
Set Ic naive. Figure 6	$1.2^{+0.9}_{-0.7}$	$-0.9^{+0.6}_{-0.8}$	$0.9^{+0.8}_{-0.6}$	$0.03^{+0.12}_{-0.08}$	$-0.05^{+0.09}_{-0.10}$
Set III naive. Figure 6	$0.5^{+0.8}_{-0.3}$	$-0.3^{+0.2}_{-0.7}$	$0.3^{+0.6}_{-0.3}$	$-0.07^{+0.18}_{-0.07}$	$-0.02^{+0.13}_{-0.07}$
Set Ic non-naive. Figure 7	$0.9^{+0.7}_{-0.6}$	$-0.7^{+0.5}_{-0.6}$	$1.0^{+1.0}_{-0.7}$	$0.1^{+0.2}_{-0.1}$	$0.08^{+0.2}_{-0.1}$
Set III non-naive. Figure 7	$0.4^{+0.7}_{-0.3}$	$-0.3^{+0.1}_{-0.6}$	$0.4^{+0.8}_{-0.4}$	$0.06^{+0.2}_{-0.1}$	$0.04^{+0.2}_{-0.1}$
Fit of Figure 8	$0.6^{+0.6}_{-0.4}$	$-0.5^{+0.3}_{-0.5}$	$0.6^{+0.7}_{-0.5}$	$0.06^{+0.1}_{-0.1}$	$0.01^{+0.1}_{-0.2}$

statistical uncertainties. Nevertheless, we quote in Tables IV and V the V_i and R_i values of Ref. [40] and Refs. [30,34], respectively, since they give an idea of how large these are violations in percentage terms.

As can be inferred from Table IV, crossing violations as introduced in Ref. [40] do not seem to be dramatically large, although this depends on their particular definition. The most serious violations appear in the V_5 rule, which combines both isospin S -wave channels and the P wave. The computed uncertainties provide a less pessimistic impression, since in some cases these violations are compatible with zero. Moreover, if the crossing violation definition of Refs. [30,34] is evaluated we see from Table V that these sum rules are better satisfied. The effect of uncertainties on the violations has been overlooked in previous work [30,31]. Nevertheless, we point out that generally speaking there are systematic, though small, crossing violations. In the partial fit scheme corresponding to Fig. 8 the crossing violations defined in Refs. [30,34] are compatible with values smaller than 0.1%.

D. Threshold parameters

The chiral expansion is expected to work best at low energies. But even so threshold parameters such as scattering lengths a_{IJ} and effective ranges b_{IJ} defined by Eq. (12) turn out to get corrections at each order of the expansion. The IAM is constructed to reproduce ChPT at all energies but in the lowest orders of the $1/f_\pi^2$ expansion. Thus, if we go to the threshold region we do not exactly reproduce the standard ChPT behavior. Nevertheless, as can be seen from the figures the difference between the standard ChPT amplitudes and the

unitarized ones is actually very small. Our results for the two-loop IAM threshold parameters are presented in Table VI. The fact that ChPT and ChPT' entries in the table are the same within errors is not accidental; it merely reflects the additive combination $\bar{b}_i = \bar{b}_i^0 + \Delta\bar{b}_i$ and the smallness of $\Delta\bar{b}_i$. A more detailed table containing the explicit separation in tree-level, one-loop, and two-loop contributions as well as 68% ellipses of the S -wave scattering lengths can be found in Ref. [23]. In general we see that the IAM threshold parameters are compatible within errors with the ChPT ones. The only exception is the slope b_{11} in the ρ channel for the two Monte Carlo schemes. The partial fit scheme provides compatible a_{11} and b_{11} values with slightly better accuracy.

E. Generalized inverse amplitude method

The Roskies sum rules provide a set of necessary conditions for a crossing symmetric $\pi\pi$ scattering amplitude. It has been noted that the IAM transforms the nonkinematical single zeros of the partial wave amplitudes into $(N+1)$ -order zeros of the IAM unitarized amplitudes, N being the order of the chiral expansion (see the denominators $[t_{IJ}^{(2)}(s)]^{N+1}$ of Eq. (20)). Since the integrals involve the interval $0 \leq s \leq 4m_\pi^2$ between the right and left hand cuts, these higher order zeros clearly influence the satisfaction of the crossing sum rules. However, there is no unique way to modify the chiral zero behavior in order to achieve a better satisfaction of crossing. To overcome this difficulty, several interesting methods have been proposed, effectively rectifying the amplitude behavior in the unphysical region, al-

 TABLE VI. Scattering lengths a_{IJ} and slopes b_{IJ} defined by Eq. (12) for the IAM and the parameter sets Ic and III of Ref. [23]. We also indicate the phase-shift figures that correspond to these threshold parameters.

	$a_{00}m_\pi$	$b_{00}m_\pi^3$	$10a_{11}m_\pi^3$	$10b_{11}m_\pi^5$	$10a_{20}m_\pi$	$10b_{20}m_\pi^3$
ChPT Ic Fig. 2	0.214(5)	0.27(1)	0.37(1)	0.06(1)	-0.42(1)	-0.76(2)
ChPT III Fig. 2	0.208(6)	0.25(1)	0.374(8)	0.053(7)	-0.44(1)	-0.80(2)
ChPT Ic Fig. 4	0.214(5)	0.27(1)	0.37(1)	0.06(1)	-0.42(1)	-0.76(2)
ChPT III Fig. 4	0.208(6)	0.25(1)	0.374(8)	0.053(7)	-0.44(1)	-0.80(2)
IAM Ic Fig. 6	0.220(7)	0.30(2)	0.37(8)	0.048(6)	-0.42(1)	-0.76(2)
IAM III Fig. 6	0.211(8)	0.27(2)	0.37(6)	0.046(5)	-0.44(1)	-0.80(2)
IAM Ic Fig. 7	0.221(8)	0.29(2)	0.38(1)	0.072(1)	-0.42(1)	-0.76(2)
IAM III Fig. 7	0.213(8)	0.27(2)	0.381(9)	0.064(1)	-0.44(1)	-0.80(2)
Fit of Fig. 8	0.216(5)	0.280(7)	0.376(6)	0.058(5)	-0.43(1)	-0.79(1)

TABLE VII. Roskies sum rules violations in percentages as defined by Eq. (27) and introduced in Ref. [40] for the generalized IAM of Ref. [34] and the parameter sets Ic and III of Ref. [23].

Generalized IAM	V_1	V_2	V_3	V_4	V_5	V_6
Set Ic naive	$-0.06^{+0.12}_{-0.11}$	$0.6^{+0.02}_{-0.09}$	$0.01^{+0.04}_{-0.04}$	$-0.02^{+0.04}_{-0.05}$	14^{+23}_{-9}	6^{+4}_{-5}
Set III naive	$0.02^{+0.01}_{-0.01}$	$0.06^{+0.02}_{-0.02}$	$0.01^{+0.03}_{-0.04}$	$-0.02^{+0.04}_{-0.04}$	8^{+10}_{-4}	2^{+4}_{-6}
Set Ic non-naive	$-0.3^{+0.1}_{-0.1}$	$-0.09^{+0.03}_{-0.04}$	$-0.04^{+0.04}_{-0.04}$	$0.02^{+0.05}_{-0.04}$	1^{+5}_{-2}	2^{+4}_{-5}
Set III non-naive	$-0.3^{+0.1}_{-0.1}$	$-0.06^{+0.03}_{-0.03}$	$-0.01^{+0.04}_{-0.03}$	$0.02^{+0.05}_{-0.04}$	1^{+2}_{-1}	2^{+4}_{-5}

though one should say that none of them is entirely satisfactory from the point of view of the mathematical properties that one wants to impose *a priori* on the amplitude. In Ref. [30] (scheme II of that work), use of a dispersion relation has been suggested for the inverse amplitude $t_{IJ}(s)^{-1}$. In this way, not only the unitarity cut but also the position of the single chiral zero, which becomes a single pole for the inverse amplitude, may be enforced from the beginning. The left hand cut is assumed to be that of ChPT up to a certain

negative $s = -\Lambda^2$ value ($\Lambda^2 = 0.5 - 0.6 \text{ GeV}^2$) and a constant up to $s = -\infty$. This procedure has the disadvantage of introducing a new variable (the cutoff Λ) into the problem not present in the ChPT amplitude. In addition, it does not take the shift in the nonkinematical chiral zeros into account, and imposes the tree-level ones. More recently, in Ref. [34] a generalized IAM to two loops was proposed. If s_0 is the chiral Adler zero to lowest order $t_{IJ}^{(2)}(s_0) = 0$ then the following expression for the inverse amplitude is suggested [34]:

$$t_{IJ}^{-1}(s) = \frac{t_{IJ}^{(2)}(s) - t_{IJ}^{(4)}(s) + t_{IJ}^{(4)}(s)^2/t_{IJ}^{(2)}(s) - t_{IJ}^{(6)}(s) + 2t_{IJ}^{(4)}(s_0)[1 - t_{IJ}^{(4)}(s)/t_{IJ}^{(2)}(s)] + 2t_{IJ}^{(6)}(s_0) + t_{IJ}^{(4)}(s_0)^2/t_{IJ}^{(2)}(s)}{[t_{IJ}^{(2)}(s) + t_{IJ}^{(4)}(s_0) + t_{IJ}^{(6)}(s_0)]^2}. \quad (28)$$

This expression violates exact unitarity since

$$\text{Im } t_{IJ}^{-1}(s) = -\sigma(s) \frac{t_{IJ}^{(2)}(s)^2 + 2t_{IJ}^{(4)}(s_0)t_{IJ}^{(2)}(s)}{[t_{IJ}^{(2)}(s) + t_{IJ}^{(4)}(s_0) + t_{IJ}^{(6)}(s_0)]^2} \quad (29)$$

and, in addition, has a single zero at the lowest order approximation of the chiral zero. The slope coincides with the one obtained in ChPT as can be seen from the formula

$$t_{IJ}(s) = [t_{IJ}^{(2)}(s_0)' + t_{IJ}^{(4)}(s_0)' + t_{IJ}^{(6)}(s_0)'](s - s_0) + \mathcal{O}[(s - s_0)^2]. \quad (30)$$

In the limit $t_{IJ}^{(4)}(s_0) + t_{IJ}^{(6)}(s_0) \rightarrow 0$ in Eq. (28) the generalized IAM of Ref. [34] reduces to the standard IAM of Eq. (20) and also unitarity is exactly satisfied. In practice, both the unitarity violations and the absence of a shift for nonkinematical zeros are numerically small. It was shown in Ref. [34] that the generalized IAM improves the satisfaction of the Roskies sum rules, but no uncertainty estimates were

considered. Using the two definitions of crossing violations given by Eqs. (26) and (27) suggested in Refs. [30,34] and [40], we show in Tables VII and VIII, respectively, that this is indeed the case, provided uncertainties in the parameters are taken into account.

IV. CONVERGENCE OF THE INVERSE AMPLITUDE METHOD

The IAM can be systematically implemented to any order in the chiral expansion with no additional LEC's other than those required by standard ChPT. There arises the question as to what extent this method is convergent. To answer this question in practice we can only compare one-loop and two loop predictions for the unitarized phase shifts. Such a comparison makes sense only if errors in the LEC's are also transported, as we have repeatedly done throughout this work. Actually, in Ref. [29] the one-loop error analysis of the IAM phase shifts was estimated by varying the low energy constants. In this section we reanalyze this question by using

TABLE VIII. Sum rule violations in percentages as defined by Eq. (26) and introduced in Refs. [30,34] for the generalized IAM of Ref. [34] and the parameter sets Ic and III of Ref. [23].

Generalized IAM	R_1	R_2	R_3	R_4	R_5
Set Ic naive	$0.08^{+0.03}_{-0.02}$	$-0.06^{+0.1}_{-0.1}$	$-0.04^{+0.09}_{-0.10}$	$-0.06^{+0.03}_{-0.03}$	$-0.05^{+0.05}_{-0.04}$
Set III naive	$0.08^{+0.02}_{-0.03}$	$0.02^{+0.1}_{-0.1}$	$-0.05^{+0.08}_{-0.09}$	$-0.03^{+0.03}_{-0.03}$	$-0.004^{+0.06}_{-0.05}$
Set Ic non-naive	$-0.11^{+0.04}_{-0.05}$	$-0.3^{+0.1}_{-0.1}$	$0.03^{+0.10}_{-0.09}$	$-0.12^{+0.03}_{-0.04}$	$-0.2^{+0.05}_{-0.06}$
Set III non-naive	$-0.08^{+0.05}_{-0.04}$	$-0.3^{+0.1}_{-0.1}$	$0.04^{+0.10}_{-0.08}$	$-0.10^{+0.03}_{-0.04}$	$-0.2^{+0.2}_{-0.1}$

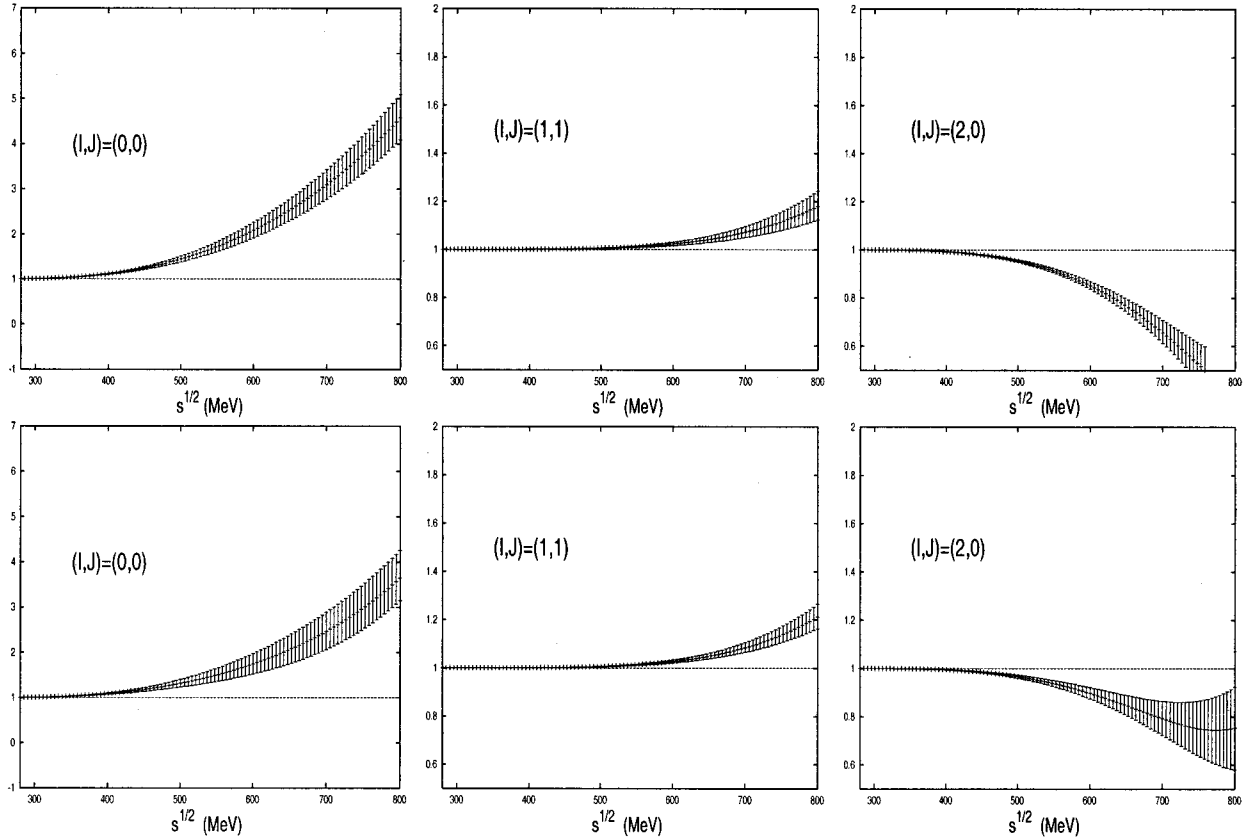


FIG. 10. Unitarity condition for standard NLO ChPT amplitudes in $\pi\pi$ scattering for S and P waves defined by $U_{IJ}(s) = |1 + 2i\sigma(s)t_{IJ}(s)|$. Upper panels: Set Ic of Ref. [23]. Lower panels: Set III of Ref. [23]. The unitarity condition requires $U_{IJ}(s) = 1$.

the updated values of the one-loop coefficients given by sets Ic and III taking into account by means of a Monte Carlo simulation the important anticorrelations between \bar{T}_1 and \bar{T}_2 determined in Ref. [23]. Following the same systematics as in the two-loop calculation, we show in Fig. 10 the unitarity condition of Eq. (9). As one would expect, unitarity violations of one-loop ChPT occur at lower energies. The NLO ChPT phase shifts defined through Eq. (10) are depicted in Fig. 11. The general trend follows a similar pattern to the two-loop calculation, although some important differences emerge. First, the uncertainties in the phase shifts are smaller at NNLO than at NLO in the threshold region, as one would expect from the fact that threshold parameters are more accurately determined at NNLO than at NLO [23].⁸ In the region above threshold the situation is exactly the opposite, the two loop calculation produces larger uncertainties than the one loop one. In addition, by comparison of Fig. 11 and Figs. 3 (and 4 in the ρ channel) one sees that the discrepancies in the region above threshold are larger than the estimated uncertainties, with an overall trend to improvement in the two-loop calculation. A similar trend, although in a less clear manner, is observed in the two S waves. The unitarity con-

dition Eq. (9) gives us a good idea about the applicability of standard ChPT to one- and two-loop approximations. Nevertheless, the agreement of the perturbative phase shifts Eq. (10) with experiment seems to extend up to a region where the unitarity violation may be as large as 10–20%.

The one-loop IAM phase shifts are depicted in Fig. 12. Clearly, the general picture provided by NLO ChPT looks better than that obtained by comparing either of the two Monte Carlo schemes studied in Sec. III based on NNLO ChPT. By looking at either of these two-loop schemes, Figs. 6 and 7, we realize that there is a clear loss of predictive power; the errors in the two-loop phase shifts are larger than the discrepancy between their mean value and the one-loop mean value. Finally, in Fig. 13 a partial one-loop fit procedure in \bar{T}_1 and \bar{T}_2 parameters to the data is presented, where variations in \bar{T}_3 and \bar{T}_4 are taken into account. The result of the fit is

$$\bar{T}_1 = -0.44 \pm 0.02, \quad \bar{T}_2 = 5.51 \pm 0.04, \quad r(\bar{T}_1, \bar{T}_2) = -0.81, \quad (31)$$

where the errors reflect the uncertainties in \bar{T}_3 and \bar{T}_4 . Here χ^2 per DOF is $191/(67-2) = 2.94$, almost three times larger than in the two-loop case (1.11), and too large to be considered a satisfactory description of the scattering data. Such a large χ^2 value makes the determination of the uncertainties of \bar{T}_1 and \bar{T}_2 due to the error bars in the fitted data mean-

⁸This circumstance is not trivial and it happens only for sets Ic and III. Set II of Ref. [23] shows cases where predictive ability in the threshold parameters is lost, and the NNLO result is no more accurate than the NLO.

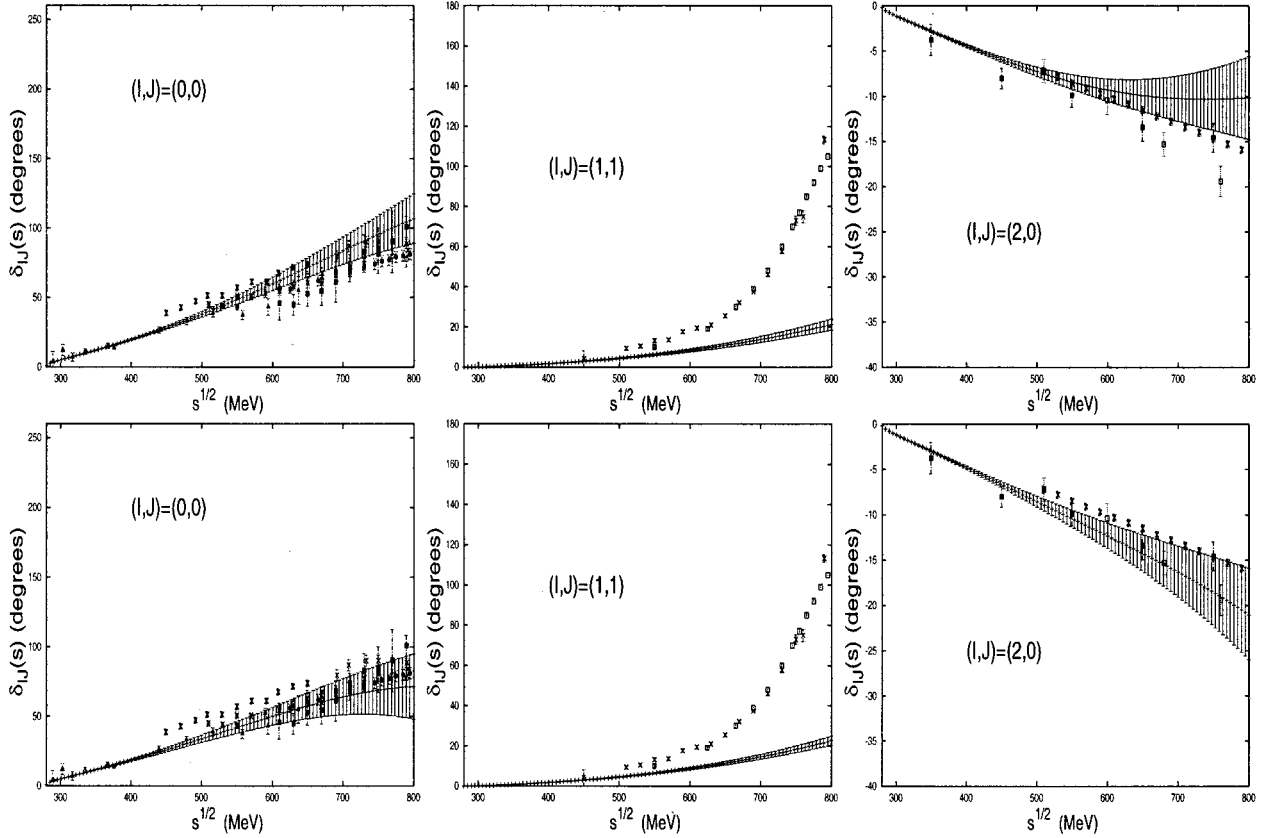


FIG. 11. Standard NLO ChPT phase shifts (in degrees) for $\pi\pi$ scattering for S and P waves after Eq. (10). Upper panels: Set Ic of Ref. [23]. Lower panels: Set III of Ref. [23]. Combined data from Refs. [2–10].

less. As we see, the values obtained for the fitted parameters are compatible with the corresponding two-loop partial fit procedure, Eq. (21), although the errors in the one-loop case due to uncertainties in \bar{I}_3 and \bar{I}_4 are much smaller than in the two-loop case. This may be an indirect consequence of the large χ^2 value.

V. CONCLUSIONS

In the present work we have presented a thorough study of the inverse amplitude method to unitarize the NLO (one-loop) and NNLO (two-loop) ChPT $\pi\pi$ scattering amplitudes below the $K\bar{K}$ threshold. To this end, we have considered several one-loop $\bar{I}_{1,2,3,4}$ and two-loop $\bar{b}_{1,2,3,4,5,6}$ parameter sets along the lines discussed in our previous work [23]. Particularly interesting in this work is the role played by the uncertainties in these parameters. To complement the analysis and provide some quantitative motivation we have determined unitarity violations within standard ChPT, with error estimates. They take place at much lower energies than the unitarity limit suggests. Moreover, we have also shown a systematic discrepancy with the data in the region above threshold if phase shifts are defined perturbatively. The discussion is complicated by the fact that the two-loop parameters $\bar{b}_{1,2,3,4,5,6}$ may be split into a zeroth order contribution $\bar{b}_{1,2,3,4,5,6}^0$ and a higher order contribution $\Delta\bar{b}_{1,2,3,4,5,6}$, which slightly spoils the chiral counting. The difference caused in

the phase shifts by including or not the higher contribution is small within ChPT. Motivated by this we have unitarized the two-loop amplitude, and devised several schemes to predict the phase shifts from threshold up to the resonance region.

The effect of consistently treating or not $\Delta\bar{b}_{1,2,3,4,5,6}$ as higher order is much stronger for the IAM unitarized phase shifts. Typically, a factor of 2 or more difference in the uncertainties is encountered. In any case, they are rather large, although they seem consistent with the scattering data. This indicates a kind of fine-tuning going on, and suggests a fit to the data to determine the low energy parameters that remain in the chiral limit, keeping the remaining low energy parameters within their error bars. The result of the fit is satisfactory, although a discrepancy appears in the \bar{b}_6 coefficient. Nevertheless, the predicted partially fitted phase shifts vary within very small uncertainties, not far from the recent ChPT analysis of the Roy equations carried out in Ref. [42]. Despite these features, the IAM produces crossing violations, which have been quantified in terms of Roskies sum rules. Generally speaking, they are not very large in percentage terms, although in some cases the uncertainties are so large that no conclusion can be drawn. We have also studied some proposals to generalize the IAM in order to achieve a better satisfaction of crossing properties. Finally, we have addressed the convergence of an expansion based on the IAM and increasing order of approximation in ChPT. By comparing NLO (one-loop) and NNLO (two-loop) IAM predicted phase shifts

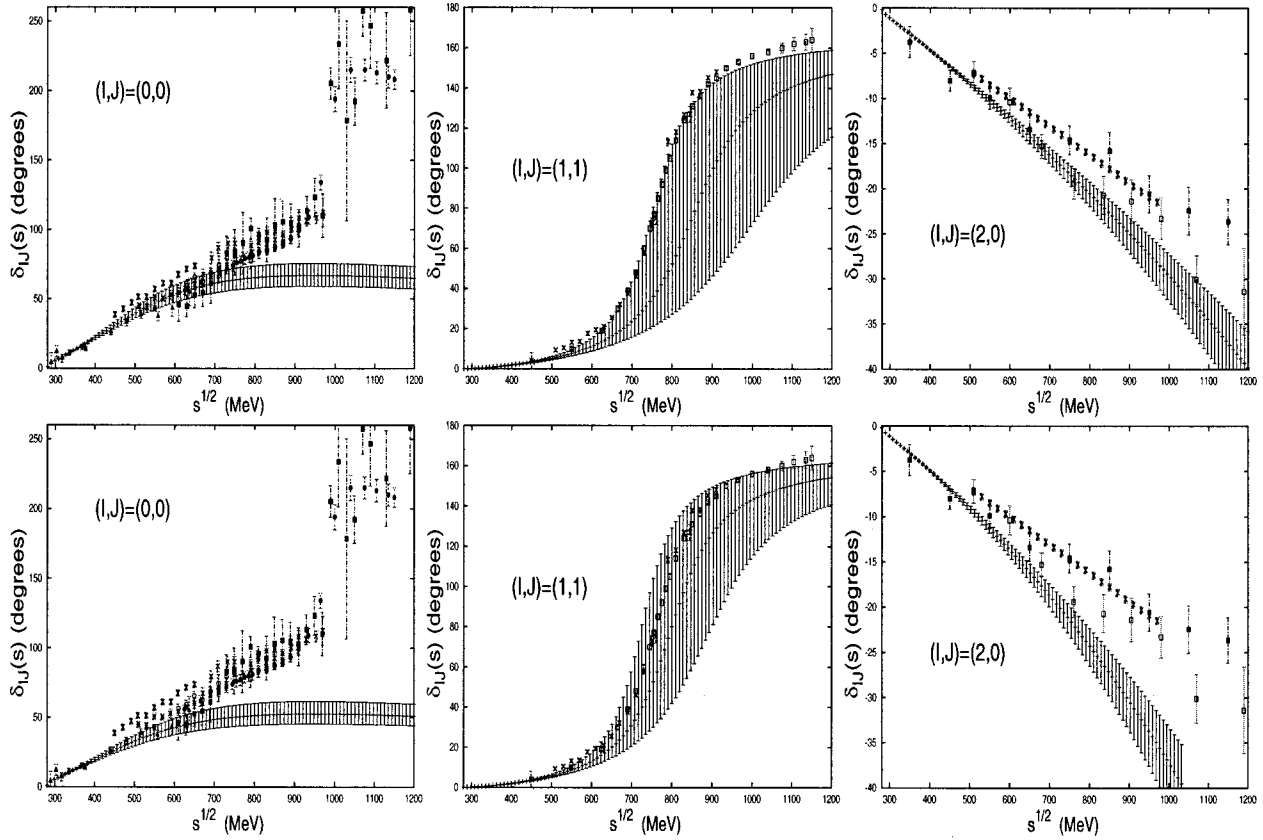


FIG. 12. NLO IAM unitarized phase shifts (in degrees) for $\pi\pi$ scattering for S and P waves. Monte Carlo scheme (see main text). Upper panels: Set Ic of Ref. [23]. Lower panels: Set III of Ref. [23]. Combined data from Refs. [2–10].

we see at the present stage a lack of predictive power; the errors in the two-loop phase shift are larger than the difference between the central one-loop and two-loop values. This is a direct consequence of the low accuracy in the two-loop parameters.

ACKNOWLEDGMENTS

This work was partially supported by DGES PB98-1367 and by the Junta de Andalucía FQM0225. The work of

M.P.V. was done in part with a grant under the auspices of the Junta de Andalucía.

APPENDIX: CORRELATIONS AMONG NEXT-TO-NEXT-TO-LEADING ORDER LOW ENERGY CONSTANTS AND THRESHOLD PARAMETERS IN STANDARD CHIRAL PERTURBATION THEORY

The correlation matrix, defined as usual by

$$r_{ij} = \langle x_i x_j \rangle, \quad (\text{A1})$$

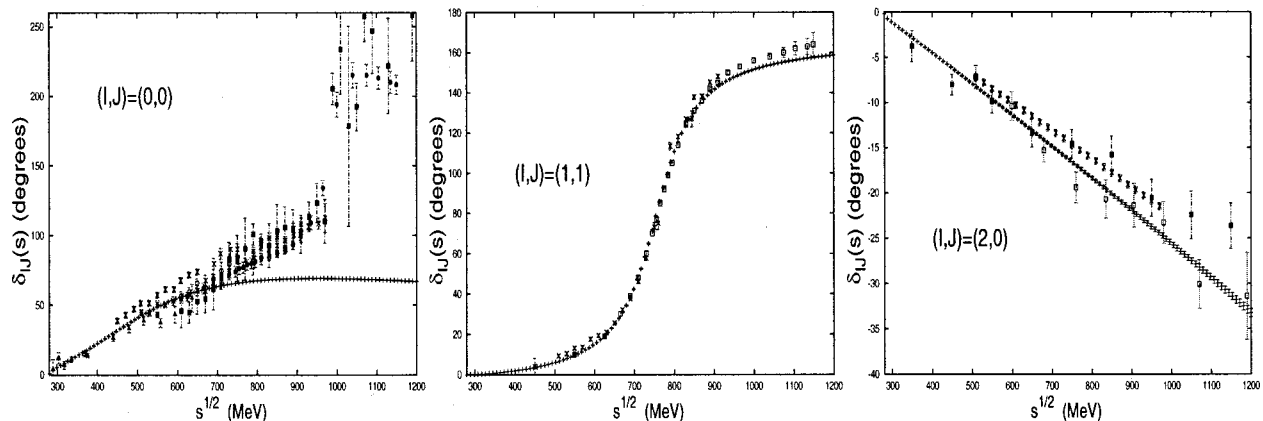


FIG. 13. NLO IAM unitarized phase shifts (in degrees) for $\pi\pi$ scattering for S and P waves. Partial fit scheme (see main text). The errors in the curves are due to uncertainties in \bar{I}_3 and \bar{I}_4 . Combined data from Refs. [2–10].

$$x_i = \frac{c_i - \langle c_i \rangle}{\sqrt{\langle c_i^2 \rangle - \langle c_i \rangle^2}},$$

$$\langle f(c_1, \dots, c_n) \rangle = \frac{1}{N} \sum_{\alpha=1}^N f(c_{1,\alpha}, \dots, c_{n,\alpha}),$$

c_i being any of the low energy constants or threshold parameters, is provided below as obtained from our $N=10^4$ finite size samples for both set Ic and set III. Taking into account the central values and their errors given in Tables II and VI and ignoring the slight error asymmetries, the parameter sets are fully general by going through diagonalization to the principal axis in parameter space and making a Monte Carlo Gaussian simulation in each principal direction.

Set Ic

$$r(\bar{b}_i, \bar{b}_j) = \begin{pmatrix} +1.00 \\ -0.74 & +1.00 \\ +0.53 & -0.77 & +1.00 \\ -0.49 & +0.64 & -0.49 & +1.00 \\ +0.09 & +0.04 & -0.41 & +0.10 & +1.00 \\ -0.08 & +0.23 & -0.54 & +0.23 & +0.57 & +1.00 \end{pmatrix}, \quad (\text{A2})$$

$$r_{ij}^{\text{threshold}} = \begin{pmatrix} a_{00} & a_{11} & a_{20} & b_{00} & b_{11} & b_{20} \\ +1.00 \\ +0.13 & +1.00 \\ +0.58 & -0.21 & +1.00 \\ +0.75 & -0.13 & +0.37 & +1.00 \\ +0.02 & +0.89 & -0.07 & -0.10 & +1.00 \\ +0.20 & +0.06 & +0.57 & +0.38 & +0.11 & +1.00 \end{pmatrix}. \quad (\text{A3})$$

Set III

$$r(\bar{b}_i, \bar{b}_j) = \begin{pmatrix} +1.00 \\ -0.73 & +1.00 \\ +0.53 & -0.76 & +1.00 \\ -0.12 & +0.20 & -0.14 & +1.00 \\ +0.22 & -0.16 & -0.19 & +0.21 & +1.00 \\ +0.06 & +0.02 & -0.29 & +0.19 & +0.47 & +1.00 \end{pmatrix}, \quad (\text{A4})$$

$$r_{ij}^{\text{threshold}} = \begin{pmatrix} a_{00} & a_{11} & a_{20} & b_{00} & b_{11} & b_{20} \\ +1.00 \\ -0.08 & +1.00 \\ +0.67 & -0.46 & +1.00 \\ +0.81 & -0.32 & +0.55 & +1.00 \\ -0.11 & +0.82 & -0.23 & -0.18 & +1.00 \\ +0.37 & -0.45 & +0.71 & +0.59 & -0.21 & +1.00 \end{pmatrix}. \quad (\text{A5})$$

[1] S. M. Roy, Phys. Lett. **36B**, 353 (1971).
 [2] S. D. Protopopescu *et al.*, Phys. Rev. D **7**, 1279 (1973).
 [3] B. Hyams *et al.*, Nucl. Phys. **B64**, 134 (1973); W. Ochs, thesis, Ludwig-Maximilians-Universität, 1973.
 [4] P. Estabrooks and A. D. Martin, Nucl. Phys. **B79**, 301 (1974).
 [5] M. J. Losty *et al.*, Nucl. Phys. **B69**, 185 (1974).
 [6] V. Srinivasan *et al.*, Phys. Rev. D **12**, 681 (1975).
 [7] L. Rosselet *et al.*, Phys. Rev. D **15**, 574 (1977).
 [8] R. Kaminski, L. Lesniak, and K. Rybicki, Z. Phys. C **74**, 79 (1997).

- [9] W. Hoogland *et al.*, Nucl. Phys. **B126**, 109 (1977).
[10] C. D. Froggatt and J. L. Petersen, Nucl. Phys. **B129**, 89 (1977).
[11] S. Weinberg, Phys. Rev. Lett. **17**, 616 (1966).
[12] J. Gasser and H. Leutwyler, Ann. Phys. (N.Y.) **158**, 142 (1984).
[13] J. Gasser and H. Leutwyler, Nucl. Phys. **B250**, 465 (1985).
[14] M. Knecht, B. Moussallam, J. Stern, and N. H. Fuchs, Nucl. Phys. **B457**, 513 (1995); **B471**, 445 (1996).
[15] J. Bijnens, G. Colangelo, G. Ecker, J. Gasser, and M. E. Sainio, Phys. Lett. B **374**, 210 (1996); Nucl. Phys. **B508**, 263 (1997); **B517**, 639(E) (1998).
[16] G. Ecker, J. Gasser, A. Pich, and E. de Rafael, Nucl. Phys. **B321**, 311 (1989).
[17] L. Girlanda, M. Knecht, B. Moussallam, and J. Stern, Phys. Lett. B **409**, 461 (1997).
[18] J. Bijnens, G. Colangelo, and J. Gasser, Nucl. Phys. **B427**, 427 (1994).
[19] G. Amoros, J. Bijnens, and P. Talavera, Phys. Lett. B **480**, 71 (2000).
[20] G. Amoros, J. Bijnens, and P. Talavera, Nucl. Phys. **B585**, 293 (2000); **B598**, 665(E) (2001).
[21] J. Bijnens, G. Colangelo, and P. Talavera, J. High Energy Phys. **05**, 014 (1998).
[22] O. Dumbrajs *et al.*, Nucl. Phys. **B216**, 277 (1983).
[23] J. Nieves and E. Ruiz Arriola, Eur. Phys. J. A **8**, 377 (2000).
[24] Tran N. Truong, Phys. Rev. Lett. **61**, 2526 (1988).
[25] A. Dobado, M. J. Herrero, and T. N. Truong, Phys. Lett. B **235**, 134 (1990).
[26] Tran N. Truong, Phys. Rev. Lett. **67**, 2260 (1991).
[27] A. Dobado and J. R. Peláez, Phys. Rev. D **47**, 4883 (1993).
[28] T. Hannah, Phys. Rev. D **54**, 4648 (1996).
[29] A. Dobado and J. R. Peláez, Phys. Rev. D **56**, 3057 (1997).
[30] M. Boglione and M. R. Pennington, Z. Phys. C **75**, 113 (1997).
[31] T. Hannah, Phys. Rev. D **55**, 5613 (1997).
[32] J. A. Oller, E. Oset, and J. R. Peláez, Phys. Rev. Lett. **80**, 3452 (1998); Phys. Rev. D **59**, 074001 (1999); **60**, 099906(E) (1999).
[33] A. Gómez Nicola and J. R. Peláez, Phys. Rev. D (to be published), hep-ph/0109056.
[34] T. Hannah, Phys. Rev. D **59**, 057502 (1999).
[35] J. Nieves and E. Ruiz Arriola, Phys. Lett. B **455**, 30 (1999).
[36] J. Nieves and E. Ruiz Arriola, Nucl. Phys. **A679**, 57 (2000).
[37] E. Ruiz Arriola, A. Gomez Nicola, J. Nieves, and J. R. Peláez, Talk given at Miniworkshop Bled 2000: Few Quark Problems, Bled, Slovenia, 2000, hep-ph/0011164.
[38] R. Roskies, Nuovo Cimento A **65**, 467 (1970).
[39] C. S. Cooper and M. R. Pennington, J. Math. Phys. **12**, 1509 (1971).
[40] I. P. Cavalcante and J. Sa Borges, hep-ph/0101037.
[41] B. Ananthanarayan, G. Colangelo, J. Gasser, and H. Leutwyler, Phys. Rep. **353**, 207 (2001), and references therein.
[42] G. Colangelo, J. Gasser, and H. Leutwyler, Nucl. Phys. **B603**, 125 (2001).
[43] T. Becher and H. Leutwyler, J. High Energy Phys. **06**, 017 (2001).